

# Rainfall Frequency Analysis Based on Long-Term High-Resolution Radar Rainfall Fields: Spatial Heterogeneities and Temporal Nonstationarities

James A. Smith<sup>1</sup>, Mary Lynn Baek<sup>1</sup>, Andrew J. Miller<sup>2</sup>, and  
Elijah L. Claggett<sup>3</sup>

<sup>1</sup>Civil & Environmental Engineering, Princeton University, 59 Olden St., Princeton, NJ 08544.

<sup>2</sup>Department of Geography and Environmental Systems, University of Maryland Baltimore County,  
Baltimore, MD 21250

<sup>3</sup>Department of Computer Science and Electrical Engineering, University of Maryland Baltimore County,  
Baltimore, MD 21250

## Key Points:

- Rainfall frequency analysis tools based on long-term, high-resolution radar rainfall fields are developed.
- Sub-daily rainfall extremes for the Baltimore study region exhibit increasing trends over 22-year period of record.
- Sub-daily rainfall extremes exhibited pronounced spatial heterogeneities over the Baltimore study region.

---

Corresponding author: James A. Smith, [jsmith@princeton.edu](mailto:jsmith@princeton.edu)

## Abstract

Rainfall frequency analyses are presented for the Baltimore Metropolitan region based on a 22-year, high-resolution radar rainfall data set. Analyses focus on spatial heterogeneities and time trends in sub-daily rainfall extremes. The rainfall data set covers a domain of 4900  $km^2$ , has a spatial resolution of approximately 1 km and a time resolution of 15 minutes. The data set combines reflectivity-based rainfall fields during the period from 2000 - 2015 and operational polarimetric rainfall fields for the period from 2012 - 2021. Analyses of rainfall fields during the 2012 - 2015 overlap period provide grounding for assessing time trends in rainfall frequency. There are pronounced spatial gradients in short-duration rainfall extremes over the study region, with peak values of rainfall between Baltimore City and Chesapeake Bay. Rainfall frequency analyses using both peaks-over-threshold and annual peak methods point to increasing trends in short-duration rainfall extremes over the period from 2000 to 2021. Intercomparisons of sub-daily rainfall extremes with daily extremes show significant differences. Less than 50% of annual maximum hourly values occur on the same day as the daily maximum and there is relatively weak correlation between magnitudes when the hourly and daily maximum overlap. Changing measurement properties are a key challenge for application of radar rainfall data sets to detection of time trends. Mean field bias correction of radar rainfall fields using rain gauge observations is both an important component of the 22-year rainfall data set and a useful tool for addressing problems associated with changing radar measurement properties.

## 1 Introduction

A cloudburst thunderstorm on 27 May 2018 produced envelope curve flood peaks in Tiber Run and devastated Ellicott City, Maryland, with rainfall accumulations that exceeded 1000 year return interval values at 3-hour time scale (Bonin et al. (2016)). The May 2018 storm was the second 1000-year rainfall event in less than two years; the 30-31 July 2016 storm produced comparable rainfall accumulations in Ellicott City at 1 - 3 hour time scale and flood peaks in Tiber Run that approached envelope curve magnitudes. These and other recent “cloudbursts” in the Mid-Atlantic have sharpened questions concerning rainfall extremes. Are short-duration rainfall extremes increasing in frequency? How do we compute rainfall frequency in a changing environment? Do rainfall extremes in Ellicott City - south and west of Baltimore - differ from rainfall extremes north and east of the urban region?

In this study, we build on a high-resolution radar rainfall data set developed for the Baltimore metropolitan region using the Hydro-NEXRAD algorithms (J. A. Smith et al. (2012); see also Krajewski et al. (2010)) with volume scan reflectivity data from the Sterling, Virginia WSR-88D (Weather Surveillance Radar - 1988 Doppler) radar covering the period 2000 - 2011. We expanded the rainfall data set by constructing rainfall fields on the same domain and grid using the operational Digital Precipitation Rate (DPR) product, which is based on polarimetric rainfall algorithms (Giangrande and Ryzhkov (2008), A. V. Ryzhkov and Zrnic (2019) and A. Ryzhkov et al. (2022)), following the polarimetric upgrade of the WSR-88D network in 2012. The DPR-based data set extends from 2012 to 2021. We also extended the Hydro-NEXRAD data set from 2012 - 2015, providing four years of overlap between the Hydro-NEXRAD and DPR data sets. The overlap period provides the observational base for comparing the two rainfall products.

Rainfall frequency analyses for short time periods have been severely limited by the sparsity of rain gauges with sub-daily measurements. High-resolution rainfall measurements from radar sample the time and space scales that rain gauge networks can not represent. They provide an important resource for rainfall frequency analyses that address sub-daily time scales, spatial heterogeneity of rainfall and changing rainfall extremes in a warming climate.

Application of radar for climatological analyses has increased over the past decade (see Saltikoff et al. (2019) for a recent review). Development of long-term data sets is a first step in creating the machinery for rainfall frequency analysis based on radar rainfall fields. Rainfall fields developed for operational weather forecasting (Nelson et al. (2016), Goudenhoofdt and Delobbe (2016), Kreklow et al. (2020), Panziera et al. (2018), and Yu et al. (2020)) provide a natural path for data-driven analyses. The “Stage IV” rainfall data set maintained by the National Weather Service has an hourly time scale and a spatial resolution of approximately 4 km over the continental US, with a record length that exceeds 20 years (2002 - 2022; Nelson et al. (2016)). Reanalysis data sets have been developed from archived radar fields and algorithms that can be tailored to climatological applications (Overeem, Holleman, and Buishand (2009), Nelson et al. (2010), Krajewski et al. (2013), J. A. Smith et al. (2012), Wright et al. (2014), Kirstetter et al. (2015), Boudevillain et al. (2016), J. Zhang et al. (2016), and Lengfeld et al. (2020)). Record lengths remain short, however, for many applications concerning rainfall and flood extremes - a central theme of methodological development for radar hydroclimatology remains “trading space for time” (e.g., Wright et al. (2020) and Andersen et al. (2022)).

Changing measurement techniques over time are an unavoidable feature of long radar rainfall data sets, especially those based on operational weather forecasting products, like the Stage IV and DPR rainfall fields. The polarimetric upgrade of the US radar network in 2012 provides an important example. In addition to changes in the basic radar measurements, operational algorithms for rainfall estimation have changed over time, as has the implementation through specification of algorithm parameters (A. Ryzhkov et al. (2022)). Addressing changes over time in hardware and algorithms used for radar rainfall estimation is an important challenge for climatological application of radar rainfall data sets, as discussed below in Section 3.

Over the past decade evidence for increasing short-duration rainfall extremes in a warming climate has mounted (Westra et al. (2014), Prein et al. (2016), and Fowler et al. (2021)). The availability of radar rainfall data sets covering the past two decades has expanded the potential for assessing climate change impacts on rainfall extremes (Saltikoff et al. (2019)). Direct assessments of changing rainfall extremes based on radar rainfall data sets provide important tools for hydroclimatological analyses.

The most direct approach to rainfall frequency analysis using gridded radar data sets is to treat observations from each grid as though they were point observations from a rain gauge. The approach underlies studies using annual maximum and peaks-over-threshold analyses for “long” radar rainfall records (Allen and DeGaetano (2005), Overeem, Buishand, and Holleman (2009), Eldardiry et al. (2015), Ghebreyesus and Sharif (2021), Marra et al. (2017), McGraw et al. (2019), Molter et al. (2021) and de Valk and Overeem (2022)). A compelling rationale for these studies is that sub-daily rain gauge networks with long records are sparse in most settings. In regions with large spatial gradients in rainfall extremes, radar provides the potential for resolving spatial heterogeneities that are difficult to address solely through gauge-based analyses (e.g. Barton et al. (2020)).

There are striking contrasts between radar and rain gauge networks in the ability to detect major rainfall events (e.g., Molter et al. (2021), Lengfeld et al. (2020) and J. A. Smith et al. (2023)). In many settings and for many storms, rain gauge networks simply do not sample extremes, especially for convective rainfall. The ability to accurately estimate extreme rainfall from radar fields, however, continues to present challenges (Schleiss et al. (2020), Peleg et al. (2018), Bárdossy and Pegram (2017), and Eldardiry et al. (2017)). Polarimetric measurements have the potential for marked improvements in rainfall estimates for climatological applications (A. Ryzhkov et al. (2022), B.-C. Seo et al. (2020), Chaney et al. (2022) and J. A. Smith et al. (2023)).

Procedures that combine radar and rain gauge observations are central to development of climatological analyses based on radar observations. They fall into two broad

categories - mean field bias adjustment (J. A. Smith and Krajewski (1991), D. J. Seo et al. (1999) and Borga et al. (2002); for recent developments, see Armon et al. (2020), B.-C. Seo et al. (2013) and Imhoff et al. (2020)) and procedures that provide spatially distributed adjustments of radar rainfall fields based on rain gauge observations (Krajewski (1987) and Creutin et al. (1988); for recent developments, see Goudenhoofdt and Delobbe (2009), Delrieu et al. (2014), Sideris et al. (2014), Ochoa-Rodriguez et al. (2019), Barton et al. (2020) and G. Zhang et al. (2021)). Mean field bias corrections are grounded in ratios of gauge observations to radar observations at rain gauge locations. Methods that provide local corrections exploit correlation structure of rainfall fields and error structure of radar rainfall fields. We use mean field bias correction as a tool for addressing changing measurement properties over the 22 year rainfall record (J. A. Smith et al. (2012)). Gauge-based mean field bias is applied as a step towards mitigating changes in measurements and algorithms.

In Section 2, we introduce data and methods, focusing on development of the 2012 - 2021 radar rainfall data set and the extreme value theory framework for rainfall frequency analysis. Climatological analyses based on the 2000 - 2021 radar rainfall data set are presented in Section 3. In Section 4, we discuss methodological issues that arise in assessing temporal nonstationarities and spatial heterogeneities of rainfall extremes using long radar rainfall data sets. We summarize the principal conclusions of our analyses in Section 5.

## 2 Data and Methods

Extreme, short-duration rainfall on 14 July 2015 produced record flooding in north Baltimore and Baltimore County (Figure 1). Peak storm total accumulations approaching 100 mm occurred over little more than an hour. Bias-corrected rainfall fields based on the Hydro-NEXRAD algorithms produced rainfall totals that closely match rainfall from the bias-corrected DPR product (Figure 1).

Rainfall fields for our study region, which is illustrated in Figure 1, cover an area of approximately  $4900 \text{ km}^2$ , with a 70 by 70 grid. Grids are 0.01 degree by 0.01 degree in size, with an area of approximately  $1 \text{ km}^2$ . For the period from 2000 - 2011, we use the bias-corrected radar rainfall fields described in J. A. Smith et al. (2012) (see also Krajewski et al. (2007)). For the period from 2012 to 2021, we utilize the operational Digital Precipitation Rate product developed by the National Weather Service based on polarimetric algorithms (Giangrande and Ryzhkov (2008) and A. Ryzhkov et al. (2022)). Like the original Hydro-NEXRAD data set for the period from 2000 - 2011, we restrict rainfall fields for the 2012 - 2021 to the months of April through September, which covers the period of peak convective rainfall. For the period from 2012 - 2015, we constructed Hydro-NEXRAD rainfall fields, using methods presented in J. A. Smith et al. (2012).

Bias correction for the DPR rainfall fields, and for the 2012 - 2015 Hydro-NEXRAD fields also follow procedures described in J. A. Smith et al. (2012). A multiplicative, mean-field bias is computed as the ratio of daily rain gauge observations to daily radar rainfall observations at gauge locations. We define a day as the 24 hour period ending at 12 UTC (7AM Eastern Standard Time), based on the climatology of convective rainfall, which exhibits a late afternoon - nighttime maximum (Ntelekos et al. (2007)).

Rain gauge observations are from networks maintained by Baltimore County and Baltimore City. Locations of rain gauges are illustrated in Figure 1. Rain gauge quality control follows procedures used for the earlier data set (J. A. Smith et al. (2012)), including outlier checks and correlation analyses among gauges.

Bias correction is an important component of rainfall estimation for the DPR rainfall fields, as was the case for the Hydro-NEXRAD rainfall fields (J. A. Smith et al. (2012)). In Figure 2, we illustrate multiplicative bias for a significant rainfall and flood event on



27 September 2018. The linear relationship between gauge and radar rainfall totals, illustrated in Figure 2, is a basic assumption underlying mean field bias correction. The bias computed for this case is 1.6.

For significant rain events, bias values are positively skewed with values larger than 1.5 occurring each year. We take significant rain events to occur on days with at least 30 positive gauges and a mean gauge rainfall greater than 20 mm for the positive gauges. Systematic monthly variation is found in bias values for significant rain events, with median values peaking around 1.5 in April and September (Table 1). During July and August, median values of bias are close to 1 and the variability of bias values, as represented by the interquartile range, is smaller than in other months. Bias values in May exhibit the largest variability over the 6 months.

The distribution of hourly rainfall rates for bias-corrected DPR and Hydro-NEXRAD for the overlap period from 2012 - 2015 are similar, especially in the upper tail (Figure 3). There are slightly larger median and .75 quantile values for DPR,  $36.6 \text{ mm h}^{-1}$  versus  $34.2 \text{ mm h}^{-1}$  and  $46.1 \text{ mm h}^{-1}$  versus  $44.7 \text{ mm h}^{-1}$ . The .25 quantile values are slightly larger for Hydro-NEXRAD,  $28.6 \text{ mm h}^{-1}$  versus  $26.8 \text{ mm h}^{-1}$ . The 0.9 quantiles are virtually identical,  $56.7 \text{ mm h}^{-1}$  for DPR versus  $56.2 \text{ mm h}^{-1}$  for Hydro-NEXRAD; for 0.99 quantiles the order switches slightly with DPR at  $97 \text{ mm h}^{-1}$  and Hydro-NEXRAD at  $98 \text{ mm h}^{-1}$ .

Range effects are an important element of the error structure of radar rainfall estimates, especially when employing observations over the full extent of the radar observations. For regional analyses, range effects are diminished, but can still contribute to rainfall estimation. We assess range effects using a simple range correction algorithm, which is based on the range-dependent frequency of 15-minute rainfall rates exceeding  $25 \text{ mm h}^{-1}$ . Additional discussion of range effects and spatial gradients of rainfall extremes is presented in Section 3.

Lightning observations from the National Lightning Detection Network (Cummins and Murphy (2009) and Orville and Huffines (2001)) are used to examine the climatology of thunderstorms in the Baltimore study region. Previous analyses of lightning climatology over the mid-Atlantic region, focusing on flash flooding in Baltimore, are presented in Ntelekos et al. (2007).

Rainfall frequency analyses are based on peaks-over-threshold and annual maximum time series at each of the 4900 grids. The modeling frameworks are introduced below.

For the peaks-over-threshold analyses, we adopt a frequency, 4 events per year on average, and determine the threshold,  $y_0$  ( $\text{mm h}^{-1}$ ), for each grid which yields the largest 88 values of rainfall for a specified duration (4 events, on average, over a 22 year period). For each grid,  $M_i$  denotes the number of events during year  $i$  exceeding threshold  $y_0$  and the magnitudes are denoted  $Y_{ij}$ ,  $j = 1, \dots, M_i$ , if  $M_i$  is greater than 0. We assume  $M_i$  has a Poisson distribution with parameter  $\lambda$ , which by construction is 4 events per year:

$$P\{M_i = k\} = \frac{\exp(-\lambda) \lambda^k}{k!} \quad (1)$$

The distribution of exceedances of  $y_0$  is assumed to have an exponential distribution:

$$G(y) = 1 - \exp\left(-\left\{\frac{y}{\sigma}\right\}\right) \quad (2)$$

The mean and standard deviation are both  $\sigma$ .

214 The annual maximum exceedance for year  $i$  is

$$\tilde{X}_i = \max \{Y_1, \dots, Y_{M_i}\} \quad (3)$$

215 if there are one or more events and 0 otherwise. The cumulative distribution function,  
 216  $P\{\tilde{X}_i \leq x\}$  is 1 minus the probability that no events exceed  $x$ , i.e.,  $P\{\sum_{j=1}^{M_i} 1(Y_{ij} > x) = 0\}$  where  $1(Y_{ij} > x)$  is 1 if  $Y_{ij} > x$  and 0 otherwise. The count of events greater  
 217 than  $x$  has a Poisson distribution with rate of occurrence that is the base rate of occur-  
 218 rence, 4 events per year, times the probability that  $Y_{ij}$  is greater than  $x$ , which is  $1 -$   
 219  $G(x)$ . It follows that, for exceedances of  $y_0$ , the quantile function is given by:  
 220

$$Q(p) = y_0 + \sigma \ln(\lambda) - \sigma \ln(-\ln(p)) \quad (4)$$

221 the quantile function of a Gumbel distribution with location  $\mu = y_0 + \sigma \ln(\lambda)$  and  
 222 scale parameter  $\sigma$ . For the T-year rainfall accumulation,  $p = 1 - \frac{1}{T}$

223 The quantile function for the time-varying form of the POT model takes the form:

$$Q_i(p) = \mu_i + \sigma_i(-\ln(-\ln(p))) \quad (5)$$

224 where the time-varying location parameter is:

$$\mu_i = y_0 + \sigma_i \ln(\lambda_i) \quad (6)$$

225  $Q_i(p)$  is the quantile function for year  $i$  and  $\mu_i$  is the location parameter for year  $i$ .

226 The annual maximum series for each grid will be denoted  $X_1, \dots, X_{22}$ ; it differs from  
 227 the POT series only for years in which the annual maximum is less than the threshold  
 228  $y_0$  used to extract peaks over threshold. We carry out extreme value analyses of the an-  
 229 nual maximum series based on the Generalized Extreme Value (GEV) distribution; its  
 230 quantile function is given by:

$$Q(p; \mu, \sigma, \xi) = \mu - \sigma \left\{ \frac{(1 - [-\ln(p)]^{-\xi})}{\xi} \right\}, \quad \xi \neq 0 \quad (7)$$

$$= \mu - \sigma \ln\{-\ln(p)\}, \quad \xi = 0 \quad (8)$$

231 In this formulation, there are three parameters, the location parameter  $\mu$ , the scale pa-  
 232 rameter  $\sigma$  and the shape parameter  $\xi$ . The Gumbel distribution is the special case for  
 233  $\xi = 0$ . The shape parameter distinguishes fundamentally different types of frequency  
 234 distributions. For positive values of the shape parameter, the distribution is unbounded  
 235 and “thick-tailed”. Negative values of the shape parameter are associated with bounded  
 236 distributions; the upper bound is given by  $\mu - \frac{\sigma}{\xi}$

237 For time-varying models based on annual maximum analyses, we assume that the  
 238 location parameter is a linear function of time :

$$\mu_i = \mu_0 + \mu_s \times Z_i \quad (9)$$

239 where the covariates  $Z_1, \dots, Z_{22}$  are time in years; in this formulation  $\mu_s$  specifies the an-  
 240 nual rate of change of the location parameter. For time-varying analyses, we focus on  
 241 Gumbel models with the assumption that the shape parameter is 0.

242 In assessing time trends, peaks-over-threshold analyses provide a different view of  
 243 nonstationarities than annual maximum analyses. Changing frequency of events,  $\lambda$ , and  
 244 changing magnitudes of events  $\sigma$  are directly assessed with peaks-over-threshold anal-  
 245 yses. For the annual maximum analyses, GEV methods focus on time changes in the lo-  
 246 cation parameter.

### 3 Climatological Analyses

How do rainfall extremes vary spatially over the Baltimore study region? The mean number of days per year with hourly rainfall accumulations greater than 25 mm has a pronounced maximum along the eastern margin of the study region, extending in an arc southeast of Baltimore to the northeast of the City along the Chesapeake Bay (Figure 4). The largest frequency is located between Baltimore City and Chesapeake Bay.

The spatial heterogeneities of hourly rainfall extremes, as illustrated in Figure 4 closely match the climatology of thunderstorm occurrence, as represented by the mean annual lightning flash density (Figure 5). Physical mechanisms for elevated thunderstorm frequency in the region are linked to interactions of the “Bay Breeze” and “Urban Heat Island” circulations. These interactions create preferential zones of surface convergence, supporting the initiation and maintenance of convective precipitation (Ryu et al. (2016)).

Spatial heterogeneities of thunderstorm occurrence exhibit a pronounced seasonal cycle (Figure 6). July and August not only have the highest frequency of thunderstorms, but also the largest spatial gradients in thunderstorm frequency. Sharp gradients in thunderstorm occurrence during July and August point to the role of land-atmosphere interactions in determining rainfall climatology. Spatial gradients in rainfall extremes over the Baltimore region (Figure 4) are closely tied to the seasonally varying climatology of thunderstorms.

The distribution of extreme rainfall rates varies markedly over the seasonal cycle from April through September. In Figure 7, we show monthly boxplots of annual maximum rainfall, given that the annual maximum is greater than 25 mm. For each month, the boxplot summarizes the distribution of annual maxima that occur in that month, based on observations from all 4900 grids. The conditional distributions increase systematically from April through August and then decrease slightly in September. August does not dominate the total number of annual maximum observations, but if an annual maximum observation occurs in August it has a more extreme upper tail than for other months.

Range correction of radar rainfall estimates (Section 2) does not qualitatively change the conclusions concerning spatial heterogeneities of extreme rainfall (Figure 4 bottom). Maximum rainfall remains concentrated along the western margin of the Chesapeake Bay, extending from southeast to northeast of the Baltimore metropolitan region.

How much information on rainfall extremes is contained in the 4900 annual maximum rainfall time series over the domain? Or, in a different formulation, how does correlation in rainfall extremes decrease with distance between grids? The spatial correlation function for annual maximum, 1 hour rainfall, was computed based on the inner 30 by 30 domain of grids. From these grids we computed the correlation from grid to grid in an east-west and in a north-south direction (Figure 8). For both, the decorrelation distance is less than 15 km. There is somewhat higher correlation in east-west direction than north-south. Both storm motion and east-west organization of convection may contribute to this feature (Ntelekos et al. (2008) and B. K. Smith et al. (2016)).

#### 3.1 Short-Duration Rainfall Extremes - “Point” Analyses

In this section we examine rainfall frequency for “points” in the study region. By point, we mean a single spatial grid cell. Analyses emulate rain gauge analyses, with each of the 4900 grid cells treated as a separate rain gauge. We begin with peaks-over-threshold analyses under the assumption of time stationarity.

The Gumbel distribution for annual maximum values is determined by the threshold  $z_0$ , the mean rate of occurrence  $\lambda$ , which is 4 per year for the stationary model, and the mean exceedance  $\sigma$ . For hourly time scale, these parameters exhibit striking spatial heterogeneity (Figure 9). Peak values of the threshold parameter extend from southwest

to northeast along the western margin of Chesapeake Bay through the Baltimore metropolitan region. The mean exceedance  $\sigma$  has a core of maximum values between Baltimore City and Chesapeake Bay. These spatial features mesh with rainfall analyses (Figure 4) and analyses of spatial heterogeneities in thunderstorm frequency (Figure 5). The 100-year rainfall at hourly time scale, based on the stationary peaks-over-threshold analyses, reflects the spatial variability of threshold and mean exceedance (Figure 9).

The east-west gradient in 100 year, hourly rainfall through Baltimore at 39.25 degrees latitude exceeds 12 mm (from more than 82 mm to less than 70 mm) over a 20 km distance (Figure 9). The NOAA precipitation frequency atlas values range from 78 mm to 77 mm over a 50 km distance through the Baltimore region at 39.25 degrees. The absence of gradients in the NOAA precipitation frequency results is not surprising; there are very few rain gauges with sub-daily accumulations. The presence of large gradients in radar analyses, which is consistent with the climatology of thunderstorms, points to the need for greater attention to spatial structure of rainfall extremes.

Time trends in rainfall extremes over the 22 year period are examined through peaks-over-threshold analyses in which the mean annual count and mean exceedance are treated as time-varying quantities. We estimate each using the Sen's slope. The distribution of slope for the rate of occurrence is strongly weighted toward increasing trends (Figure 10); 75% of the grids have positive slopes. For the mean exceedance, 50% of grids have positive slopes. The distribution of slopes, however, is skewed to large positive values concentrated around Baltimore City and Chesapeake Bay (Figure 10).

Using the Sen slope for the rate of occurrence and mean exceedance, we constructed Gumbel model parameters (Equations 5 and 6) for the year 2000 and for the year 2021. From these parameters we computed quantiles of hourly rainfall at the beginning and end of the 22 year time period. In Figure 11, we show the 2021 distribution of 100-year, 1 hour rainfall rates for the 4900 grids (top) and the ratio of the 2021 100-year return interval value to the 2000 value. The median value of 100-year ratio is 1.09 and 88 % of grids have values larger than 1 (Figure 12).

Over Baltimore City, the 100-year hourly rain increases from 62 mm to 74 mm over the 22-year period. The change in 100-year rainfall over a 22-year time period is comparable to the "spatial" change in 100-year rainfall over a 20 km east-west transect, as detailed above.

Analyses of short-duration rainfall extremes based on the annual maximum formulation (Equations 7 - 10) provide similar conclusions and additional insights concerning time trends over the 22-year period. Parameters of a Gumbel distribution in which the location is a linear function of year were estimated for each of the 4900 grids. In Figure 13, we show the distribution of 100-year, 1 hour rainfall rates for the 4900 grids (top) and the ratio of the 2021 100-year return interval value to the 2000 value, based on the Gumbel model with linear time trends in the location parameter. The median value of the ratio between 2021 and 2000 rainfall magnitudes is 1.09 and 87 % of grids have values larger than 1. Extreme value analyses based on annual maximum observations point to increasing short-duration rainfall extremes.

For the annual maximum series, we also examined rainfall frequency based on a GEV model in which the shape parameter is not constrained to be 0, as is the case for the Gumbel distribution. For the stationary model, GEV analyses provide non-physical values of the shape parameter for some grids. More than 250 grids have estimated shape values larger than 0.5, implying a distribution with infinite variance. For 25% of the grids, the shape parameter is larger than 0.25. Large values of the shape parameter are principally due to annual maximum series in which the record rainfall is much larger than the other 21 values. Several storm events are responsible for large record rainfall values and non-physical shape parameters. Record length for radar rainfall data sets, includ-

ing the Baltimore data set, does not support application of GEV models in which the shape parameter is estimated.

### 3.2 Daily versus Short-Duration Rainfall Extremes

Are the key features of sub-daily rainfall extremes represented through analyses of daily annual maxima? In most settings, long sub-daily records are sparse. Consequently, there is considerable attention given to daily analyses, with inferences that results developed from daily analyses apply to sub-daily extremes. If, for example, the 100-year daily rainfall increases by 10%, can we assume that hourly rainfall increases by the same amount?

For each of the 4900 grids, we examined the relationships between daily and sub-daily rainfall extremes based on annual maximum records. A basic question is whether the annual maximum hourly rainfall values are embedded in the annual maximum daily rainfall. Does the annual maximum hourly rainfall occur on the day of the annual maximum daily rainfall? At the hourly time scale, fewer than 50 per cent of annual maximum hourly observations occur on the same day as the daily maximum.

There is spatial structure to the relationship between the joint occurrence of daily and hourly annual maxima (Figure 14). The highest frequency is along Chesapeake Bay, a region in which hourly extremes are prominent in August (Figures 6 and 7). Hourly and daily extremes are more closely linked in the region in which convective rainfall is most prominent.

The joint distributions of hourly and daily annual maxima for years in which they occur on the same day are flat for a broad range of daily rainfall accumulation (Figure 15). Even for years in which the maximum hourly rainfall occurs on the same day as the daily max, the two are not strongly related.

### 3.3 Short-Duration Rainfall Extremes - Spatial Analyses

An advantage of radar for rainfall frequency analyses is the ability to directly examine spatially-averaged rainfall extremes. In this section, we present Gumbel analyses of annual maximum rainfall time series constructed from spatial averaging of radar rainfall fields. In particular, we examine rainfall averaged over 3 by 3 grids - approximately  $9 \text{ km}^2$  - 5 by 5 grids approximately  $25 \text{ km}^2$  and 10 by 10 grids - approximately  $100 \text{ km}^2$ .

Analyses of time trends largely follow the “point” results ( $1 \text{ km}^2$ ) from the previous section. In Figure 16, we show 100-year, 1 hour rainfall over  $100 \text{ km}^2$  area for 2021 (top) and the ratio of 2021 values to 2000 values (bottom). The distribution of 100-year rainfall values in 2021 is asymmetric, with longer tails on the low end of the distribution.

The median values of 100 year, 1 hour rainfall in 2021 decreases from 78 mm at  $1 \text{ km}^2$  scale to 58 mm at  $100 \text{ km}^2$  scale (Table 2). For all spatial scales, the percentage of grids with increasing time trends exceeds 87%. The evidence for nonstationarity increases with averaging area; at  $100 \text{ km}^2$  scale, 91% of grids have slopes greater than 1.

## 4 Summary and Conclusions

We present rainfall frequency analyses from a 22-year radar rainfall data set covering a  $4900 \text{ km}^2$  domain around the Baltimore metropolitan region. Analyses focus on spatial gradients and time trends in short-duration rainfall extremes. The principal conclusions are summarized below.

- There are pronounced spatial gradients in short-duration rainfall extremes over the study region, with peak values of rainfall between Baltimore City and Chesapeake Bay. Spatial gradients in short-duration extremes based on radar rainfall analyses closely match the climatology of thunderstorms, as reflected in climatological analyses of lightning flash density based on NLDN observations. Spatial gradients in rainfall extremes and lightning climatology are consistent with physical mechanisms tied to interactions between the Urban Heat Island circulation and Bay Breeze circulation, as detailed in Ryu et al. (2016). Spatial gradients in short-duration rainfall extremes are not reflected in NOAA Atlas 14 products.
- Analyses of short-duration rainfall extremes through both peaks-over-threshold and annual analyses using the 22-year rainfall data set point to increasing trends. Peaks-over-threshold analyses point to spatial contrasts in changes in rate of occurrence and magnitudes of threshold exceedance. Analyses of time trends based on radar rainfall data sets are fundamentally limited by record length. Changes in magnitudes of threshold exceedance are particularly important for changing extremes. Distinguishing climate variability at decadal time scales from climate change (e.g., Kunkel et al. (2013) and Martel et al. (2018)) is an important challenge for analyses based on long radar rainfall data sets.
- Analyses of time trends for spatially-averaged rainfall show results that are similar to the “point” analyses based on 1 km grids. An important advantage of radar rainfall fields for rainfall frequency analysis is the ability to directly examine frequency for spatially-averaged rainfall.
- Intercomparisons of sub-daily rainfall extremes with daily extremes show significant differences. Less than 50 % of annual maximum hourly values occur on the same day as the daily max. In years when the hourly maximum occurs on the same day as the daily maximum, there is relatively weak correlation between the magnitudes. The assumption that sub-daily rainfall extremes are closely linked to daily extremes warrants additional consideration, especially for development of new rainfall frequency approaches that account for the impacts of climate change.
- Rainfall frequency analyses based on the GEV distribution suffer from “non-physical” values of the shape parameter. The limited sample size of radar rainfall data sets does not support application of the GEV with shape as a free parameter.
- Changing measurement environments are a key challenge for application of radar rainfall data sets to detection of time trends. A significant change in the Baltimore data set is the transition to polarimetric estimates in 2012. Intercomparisons of rainfall fields based on reflectivity algorithms (Hydro-NEXRAD) and polarimetric algorithms (DPR) during the overlap period from 2012 - 2015 point to a generally good match.
- Mean field bias correction of radar rainfall fields using rain gauge observations is both an important component of the 22-year rainfall data set and a tool for mitigating the effects of changing radar measurement properties. For the polarimetric era, there is pronounced variation in mean field bias for major rainfall events, with values larger than 1.5 occurring multiple times every year. There is pronounced seasonal variation in bias values, with the largest values during April and September; values during July and August are more closely clustered around 1.0. Mean field bias correction provides a useful tool for dealing with changing measurement technologies and algorithms.
- Range correction is an important component of climatological analyses of radar rainfall fields, especially for assessing spatial gradients over the full domain covered by the radar. Regional analyses, like those presented in this study for the Baltimore study area, diminish but do not eliminate the problem. Range correction for the Baltimore region does not qualitatively alter conclusions concerning spatial gradients in short-duration rainfall extremes. Additional analyses of range correction algorithms are needed for assessing spatial gradients of short-duration rainfall extremes using radar rainfall data sets.



This research was supported by the National Science Foundation (EAR-1632048) and NOAA Cooperative Institute for Modeling the Earth System. NLDN data were provided by the NASA Goddard Space Flight Center through an agreement with Vaisala Inc.

**Data Availability** - Radar rainfall fields and rain gauge data sets used for analyses in this paper will be available through the CUAHSI HydroShare portal.

## References

- Allen, R. J., & DeGaetano, A. T. (2005). Considerations for the use of radar-derived precipitation estimates in determining return intervals for extreme areal precipitation amounts. *Journal of Hydrology*, 315(1-4), 203–219.
- Andersen, C. B., Wright, D. B., & Thorndahl, S. (2022). Sub-Hourly to Daily Rainfall Intensity-Duration-Frequency Estimation Using Stochastic Storm Transposition and Discontinuous Radar Data. *Water*, 14(24), 4013.
- Armon, M., Marra, F., Enzel, Y., Rostkier-Edelstein, D., & Morin, E. (2020). Radar-based characterisation of heavy precipitation in the eastern Mediterranean and its representation in a convection-permitting model. *Hydrology and Earth System Sciences*, 24(3), 1227–1249.
- Bárdossy, A., & Pegram, G. (2017). Combination of radar and daily precipitation data to estimate meaningful sub-daily point precipitation extremes. *Journal of Hydrology*, 544, 397–406.
- Barton, Y., Sideris, I. V., Raupach, T. H., Gabella, M., Germann, U., & Martius, O. (2020). A multi-year assessment of sub-hourly gridded precipitation for Switzerland based on a blended radar–Rain-gauge dataset. *International Journal of Climatology*, 40(12), 5208–5222.
- Bonin, G. M., Martin, D., Lin, B., Parzybok, T., Yetka, M., & Riley, D. (2016). *NOAA Atlas 14: Precipitation Frequency Atlas of the United States, Volume 2 Version 3.0* (Tech. Rep.). Silver Spring, Maryland: National Weather Service.
- Borga, M., Tonelli, F., Moore, R. J., & Andrieu, H. (2002). Long-term assessment of bias adjustment in radar rainfall estimation. *Water Resources Research*, 38(11). (doi:10.1029/2001WR000555)
- Boudevillain, B., Delrieu, G., Wijbrans, A., & Confoland, A. (2016). A high-resolution rainfall re-analysis based on radar–raingauge merging in the Cévennes-Vivarais region, France. *Journal of Hydrology*, 541, 14–23.
- Chaney, M. M., Smith, J. A., & Baeck, M. L. (2022). Range Dependence of Polarimetric Radar Estimates for Extreme Flood-Producing Rainfall in Urban Watersheds. *Journal of Hydrometeorology*, 23(8), 1205–1226.
- Creutin, J., Delrieu, G., & Lebel, T. (1988). Rain measurement by raingage-radar combination: a geostatistical approach. *Journal of Atmospheric and Oceanic Technology*, 5(1), 102–105.
- Cummins, K. L., & Murphy, M. J. (2009). An overview of lightning locating systems: History, techniques, and data uses, with an in-depth look at the US NLDN. *IEEE transactions on electromagnetic compatibility*, 51(3), 499–518.
- Delrieu, G., Wijbrans, A., Boudevillain, B., Faure, D., & Kirstetter, P.-E. (2014). Geostatistical radar–raingauge merging: A novel method for the quantification of rain estimation accuracy. *Advances in Water Resources*, 71, 110–124.
- de Valk, C., & Overeem, A. (2022). A simple model for predicting the statistics of spatiotemporal extremes of sub-daily precipitation. *Weather and Climate Extremes*, 36, 100424.
- Eldardiry, H., Habib, E., & Zhang, Y. (2015). On the use of radar-based quantitative precipitation estimates for precipitation frequency analysis. *Journal of Hydrology*, 531, 441–453.
- Eldardiry, H., Habib, E., Zhang, Y., & Grashel, J. (2017). Artifacts in Stage IV

- NWS real-time multisensor precipitation estimates and impacts on identification of maximum series. *Journal of Hydrologic Engineering*, 22(5), E4015003.
- Fowler, H. J., Ali, H., Allan, R. P., Ban, N., Barbero, R., Berg, P., . . . others (2021). Towards advancing scientific knowledge of climate change impacts on short-duration rainfall extremes. *Philosophical Transactions of the Royal Society A*, 379(2195), 20190542.
- Ghebreyesus, D. T., & Sharif, H. O. (2021). Development and Assessment of High-Resolution Radar-Based Precipitation Intensity-Duration-Curve (IDF) Curves for the State of Texas. *Remote Sensing*, 13(2890), <https://doi.org/10.3390/rs13152890>.
- Giangrande, S. E., & Ryzhkov, A. V. (2008). Estimation of rainfall based on the results of polarimetric echo classification. *Journal of Applied Meteorology and Climatology*, 47, 2445 - 2462.
- Goudenhoofdt, E., & Delobbe, L. (2009). Evaluation of radar-gauge merging methods for quantitative precipitation estimates. *Hydrology and Earth System Sciences*, 13(2), 195–203.
- Goudenhoofdt, E., & Delobbe, L. (2016). Generation and verification of rainfall estimates from 10-yr volumetric weather radar measurements. *Journal of Hydrometeorology*, 17(4), 1223–1242.
- Imhoff, R., Brauer, C., Overeem, A., Weerts, A., & Uijlenhoet, R. (2020). Spatial and temporal evaluation of radar rainfall nowcasting techniques on 1,533 events. *Water Resources Research*, 56(8), Spatial and temporal evaluation of radar rainfall nowcasting techniques on 1,533 events.
- Kirstetter, P.-E., Gourley, J. J., Hong, Y., Zhang, J., Moazamigoodarzi, S., Langston, C., & Arthur, A. (2015). Probabilistic precipitation rate estimates with ground-based radar networks. *Water Resources Research*, 51(3), 1422 – 1442.
- Krajewski, W. F. (1987). Cokriging radar-rainfall and rain gage data. *Journal of Geophysical Research - Atmospheres*, 92(D8), 9571–9580.
- Krajewski, W. F., Kruger, A., Lawrence, R., Smith, J. A., Bradley, A. A., Steiner, M., . . . Goska, R. (2007). Towards better utilization of NEXRAD data in hydrology: An overview of Hydro-NEXRAD. In K. C. Kabbes (Ed.), (Vol. 243, p. 288-288). ASCE.
- Krajewski, W. F., Kruger, A., Singh, S., Seo, B.-C., & Smith, J. A. (2013). Hydro-NEXRAD-2: Real-time access to customized radar-rainfall for hydrologic applications. *Journal of Hydroinformatics*, 15(2), 580–590.
- Krajewski, W. F., Kruger, A., Smith, J. A., Lawrence, R., Gunyon, C., Goska, R., . . . Steiner, M. (2010). Towards better utilization of NEXRAD data in hydrology: An overview of Hydro-NEXRAD. *Journal of Hydroinformatics*, 13.2, 255-266.
- Kreklow, J., Tetzlaff, B., Burkhard, B., & Kuhnt, G. (2020). Radar-Based Precipitation Climatology in Germany—Developments, Uncertainties and Potentials. *Atmosphere*, 11(2), 217.
- Kunkel, K. E., Karl, T. R., Brooks, H., Kossin, J., Lawrimore, J. H., Arndt, D., . . . others (2013). Monitoring and understanding trends in extreme storms: state of the knowledge. *Bulletin of the American Meteorological Society*, 94, 499 - 514.
- Lengfeld, K., Kirstetter, P.-E., Fowler, H. J., Yu, J., Becker, A., Flamig, Z., & Gourley, J. (2020). Use of radar data for characterizing extreme precipitation at fine scales and short durations. *Environmental Research Letters*, 15(8), 085003.
- Marra, F., Morin, E., Peleg, N., Mei, Y., & Anagnostou, E. N. (2017). Intensity-duration-frequency curves from remote sensing rainfall estimates: comparing satellite and weather radar over the eastern Mediterranean. *Hydrology and Earth System Sciences*, 21(5), 2389–2404.
- Martel, J.-L., Mailhot, A., Brissette, F., & Caya, D. (2018). Role of natural climate

- variability in the detection of anthropogenic climate change signal for mean and extreme precipitation at local and regional scales. *Journal of Climate*, 31(11), 4241–4263.
- McGraw, D., Nikolopoulos, E. I., Marra, F., & Anagnostou, E. N. (2019). Precipitation frequency analyses based on radar estimates: An evaluation over the contiguous United States. *Journal of Hydrology*, 573, 299–310.
- Molter, E. M., Collins, W. D., & Risser, M. D. (2021). Quantitative precipitation estimation of extremes in conus with radar data. *Geophysical Research Letters*, 48(16), e2021GL094697.
- Nelson, B. R., Prat, O. P., Seo, D.-J., & Habib, E. (2016). Assessment and implications of NCEP Stage IV quantitative precipitation estimates for product intercomparisons. *Weather and Forecasting*, 31(2), 371–394.
- Nelson, B. R., Seo, D., & Kim, D. (2010). Multisensor precipitation reanalysis. *Journal of Hydrometeorology*, 11(3), 666–682.
- Ntelekos, A. A., Smith, J. A., Baek, M. L., Krajewski, W. F., Miller, A. J., & Goska, R. (2008). Extreme hydrometeorological events and the urban environment: Dissecting the 7 July 2004 thunderstorm over the Baltimore, MD, metropolitan region. *Water Resources Research*, 44(W08446). (doi:10.1029/2007WR006346)
- Ntelekos, A. A., Smith, J. A., & Krajewski, W. F. (2007). Climatological analyses of thunderstorms and flash floods in the Baltimore Metropolitan region. *Journal of Hydrometeorology*, 8, 88–101.
- Ochoa-Rodriguez, S., Wang, L.-P., Willems, P., & Onof, C. (2019). A review of radar-rain gauge data merging methods and their potential for urban hydrological applications. *Water Resources Research*, 55(8), 6356–6391.
- Orville, R. E., & Huffines, G. R. (2001). Cloud-to-ground lightning in the United States: NLDN results in the first decade, 1989–98. *Monthly Weather Review*, 129, 1179–1193.
- Overeem, A., Buishand, A., & Holleman, I. (2009). Extreme rainfall analysis and estimation of depth-duration-frequency curves using weather radar. *Water Resources Research*, 45(W10424). (doi:10.1029/2009WR007869)
- Overeem, A., Holleman, I., & Buishand, A. (2009). Derivation of a 10-year radar-based climatology of rainfall. *Journal of Applied Meteorology and Climatology*, 48, 1448–1463.
- Panziera, L., Gabella, M., Germann, U., & Martius, O. (2018). A 12-year radar-based climatology of daily and sub-daily extreme precipitation over the Swiss Alps. *International Journal of Climatology*, 38(10), 3749–3769.
- Peleg, N., Marra, F., Fatichi, S., Paschalis, A., Molnar, P., & Burlando, P. (2018). Spatial variability of extreme rainfall at radar subpixel scale. *Journal of Hydrology*, 556, 922–933.
- Prein, A. F., Rasmussen, R. M., Ikeda, K., Liu, C., Clark, M. P., & Holland, G. J. (2016). The future intensification of hourly precipitation extremes. *Nature Climate Change*, DOI:10.1038/NCLIMATE3168.
- Ryu, Y.-H., Smith, J. A., Bou-Zeid, E., & Baek, M. L. (2016). The influence of land surface heterogeneities on heavy convective rainfall in the Baltimore-Washington Metropolitan Area. *Monthly Weather Review*, 144, 553–573.
- Ryzhkov, A., Zhang, P., Bukovčić, P., Zhang, J., & Cocks, S. (2022). Polarimetric Radar Quantitative Precipitation Estimation. *Remote Sensing*, 14(7), 1695.
- Ryzhkov, A. V., & Zrnica, D. S. (2019). *Radar Polarimetry for Weather Observations*. Springer.
- Saltikoff, E., Friedrich, K., Soderholm, J., Lengfeld, K., Nelson, B., Becker, A., ... Tassone, C. (2019). An overview of using weather radar for climatological studies: successes, challenges, and potential. *Bulletin of the American Meteorological Society*, 100(9), 1739–1752.
- Schleiss, M., Olsson, J., Berg, P., Niemi, T., Kokkonen, T., Thorndahl, S., ...

- Pulkkinen, S. (2020). The accuracy of weather radar in heavy rain: a comparative study for Denmark, the Netherlands, Finland and Sweden. *Hydrology and Earth System Sciences*, 24(6), 3157–3188.
- Seo, B.-C., Cunha, L. K., & Krajewski, W. F. (2013). Uncertainty in radar-rainfall composite and its impact on hydrologic prediction for the eastern Iowa flood of 2008. *Water Resources Research*, 49(5), 2747–2764.
- Seo, B.-C., Krajewski, W. F., & Ryzhkov, A. (2020). Evaluation of the specific attenuation method for radar-based quantitative precipitation estimation: Improvements and practical challenges. *Journal of Hydrometeorology*, 21(6), 1333–1347.
- Seo, D. J., Breidenbach, J. P., & Johnson, E. R. (1999). Real-time estimation of mean field bias in radar rainfall data. *Journal of Hydrology*, 223(3–4), 131–147.
- Sideris, I., Gabella, M., Erdin, R., & Germann, U. (2014). Real-time radar-rain-gauge merging using spatio-temporal co-kriging with external drift in the alpine terrain of Switzerland. *Quarterly Journal of the Royal Meteorological Society*, 140(680), 1097–1111.
- Smith, B. K., Smith, J., & Baeck, M. L. (2016). Flash flood-producing storm properties in a small urban watershed. *Journal of Hydrometeorology*, 17(10), 2631–2647.
- Smith, J. A., Back, M. L., Su, Y., Vecchi, G. A., & Liu, M. (2023). “Strange Storms”: Extreme rainfall from the remnants of Hurricane Ida (2021) in the Northeastern US. *Water Resources Research*, 59(3), e2022WR033934 (<https://doi.org/10.1029/2022WR033934>).
- Smith, J. A., Baeck, M. L., Villarini, G., C.Welty, Miller, A. J., & Krajewski, W. F. (2012). Analyses of a long-term high-resolution radar rainfall data set for the Baltimore metropolitan region. *Water Resources Research*, 48(4).
- Smith, J. A., & Krajewski, W. F. (1991). Estimation of the mean field bias of radar rainfall estimates. *Journal of Applied Meteorology*, 30, 397–412.
- Westra, S., Fowler, H. J., Evans, J. P., Alexander, L. V., Berg, P., Johnson, F., ... Roberts, N. M. (2014). Future changes to the intensity and frequency of short-duration rainfall. *Reviews of Geophysics*, 52(3), 522 - 555.
- Wright, D. B., Smith, J. A., Villarini, G., & Baeck, M. L. (2014). Long-term high-resolution radar rainfall fields for urban hydrology. *Journal of the American Water Resources Association*, 50(3), 713–734.
- Wright, D. B., Yu, G., & England Jr., J. F. (2020). Six Decades of Rainfall and Flood Frequency Analysis Using Stochastic Storm Transposition: Review, Progress, and Prospects. *Journal of Hydrology*, 585, 124816.
- Yu, J., Li, X.-F., Lewis, E., Blenkinsop, S., & Fowler, H. J. (2020). UKGrSHP: a UK high-resolution gauge-radar-satellite merged hourly precipitation analysis dataset. *Climate Dynamics*, 54(5), 2919–2940.
- Zhang, G., Tian, G., Cai, D., Bai, R., & Tong, J. (2021). Merging radar and rain gauge data by using spatial-temporal local weighted linear regression kriging for quantitative precipitation estimation. *Journal of Hydrology*, 601, 126612.
- Zhang, J., Howard, K., Langston, C., Kaney, B., Qi, Y., Tang, L., ... others (2016). Multi-Radar Multi-Sensor (MRMS) quantitative precipitation estimation: Initial operating capabilities. *Bulletin of the American Meteorological Society*, 97(4), 621–638.

**Table 1.** Quantiles of bias values by month; top row is .25 quantile, second row is .50 quantile (median) and third row is the .75 quantile. Results are for days with more than 30 positive pairs and mean gauge rainfall for positive gauges exceeding 20 mm. Final row gives number of days by month satisfying the 30 pair / 20 mm criterion.

	<i>April</i>	<i>May</i>	<i>June</i>	<i>July</i>	<i>August</i>	<i>September</i>
.25	1.26	0.92	0.93	0.92	1.01	1.04
.50	1.51	1.27	1.13	1.01	1.07	1.29
.75	1.76	1.82	1.25	1.20	1.19	1.61
Count	12	17	17	19	13	13

**Table 2.** Median value of the 100-year rainfall and per cent of grids with slopes greater than 1 for specified durations and averaging area.

	Median (mm)	Per Cent
1 hour - 1 $km^2$	78	87
1 hour - 9 $km^2$	72	88
1 hour - 25 $km^2$	68	89
1 hour - 100 $km^2$	58	91



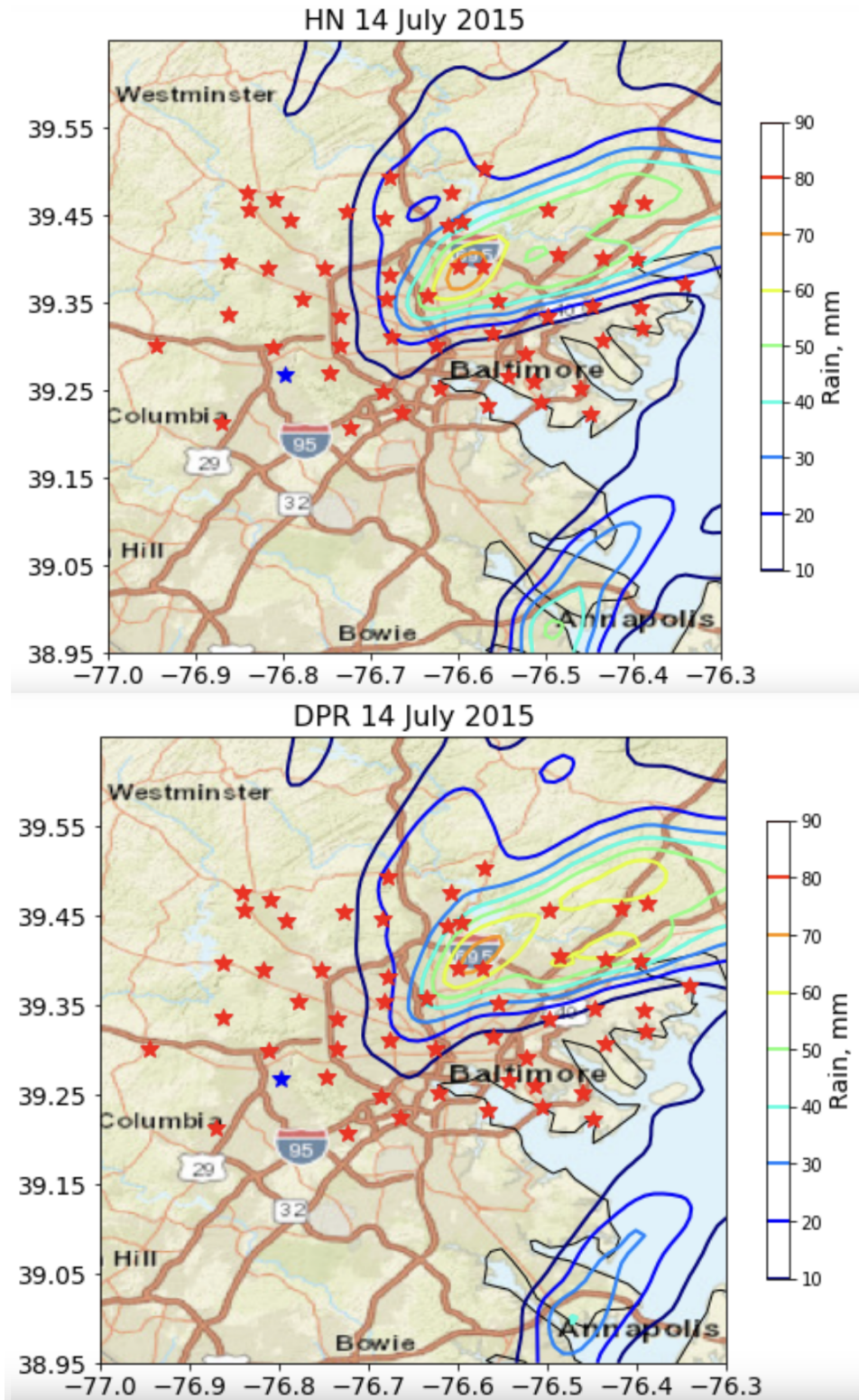


**Figure 1.** Storm total rainfall (mm) for 14 July 2015 from Hydro-NEXRAD (top) and DPR (bottom) with locations of Baltimore County and Baltimore City rain gauges (red stars). Ellicott City rain gauge is marked by a blue star.



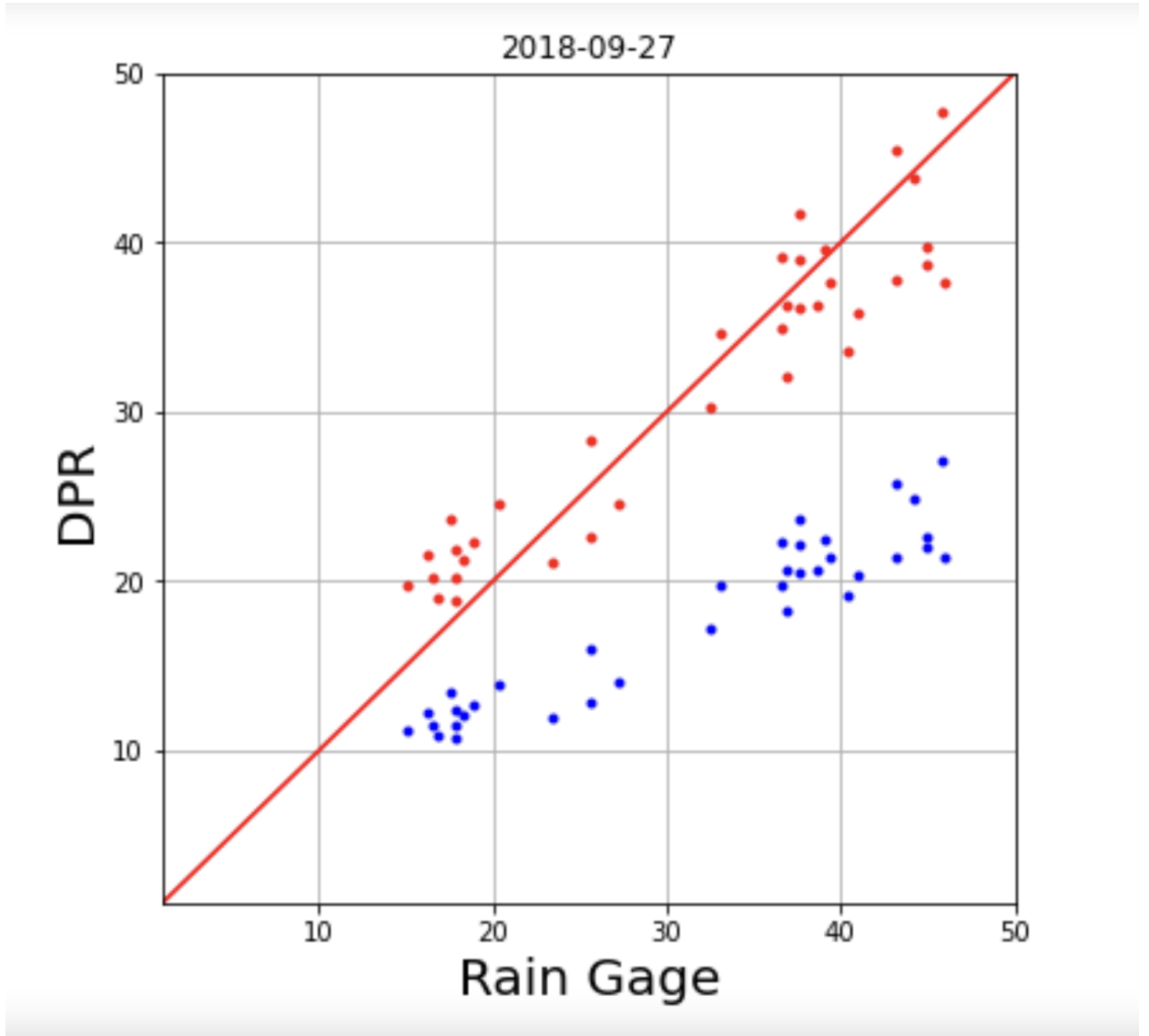


**Figure 2.** Scatterplot of storm total rainfall accumulations (mm) for 27 September 2018 from rain gauge and DPR (blue circles). Bias-corrected DPR accumulations are shown in red. The 1 to 1 line is shown in red.

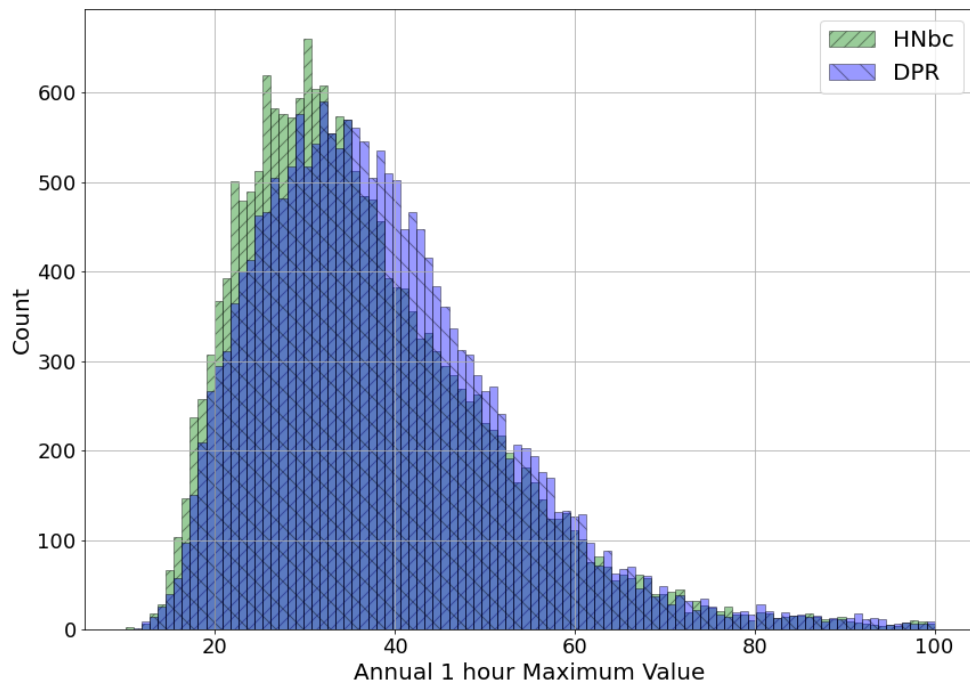


**Figure 3.** Histograms of annual maximum rainfall values from bias-corrected DPR and Hydro-NEXRAD (HNbc) analyses for the period 2012 - 2015.

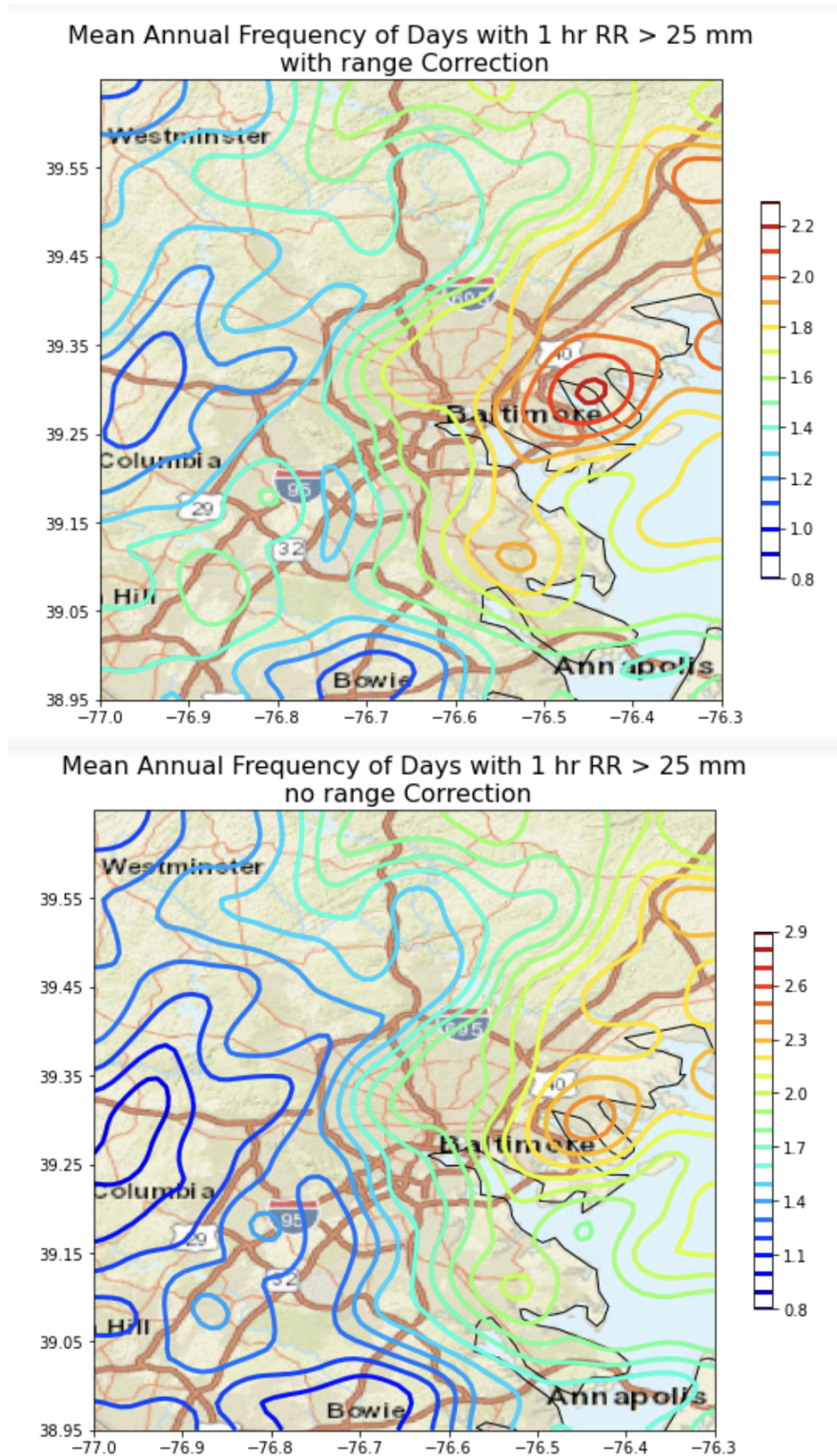


**Figure 4.** Mean number of days per year with hourly rain greater than 25 mm based on DPR rainfall fields. Top figure is with range correction; the bottom figure is without range correction.

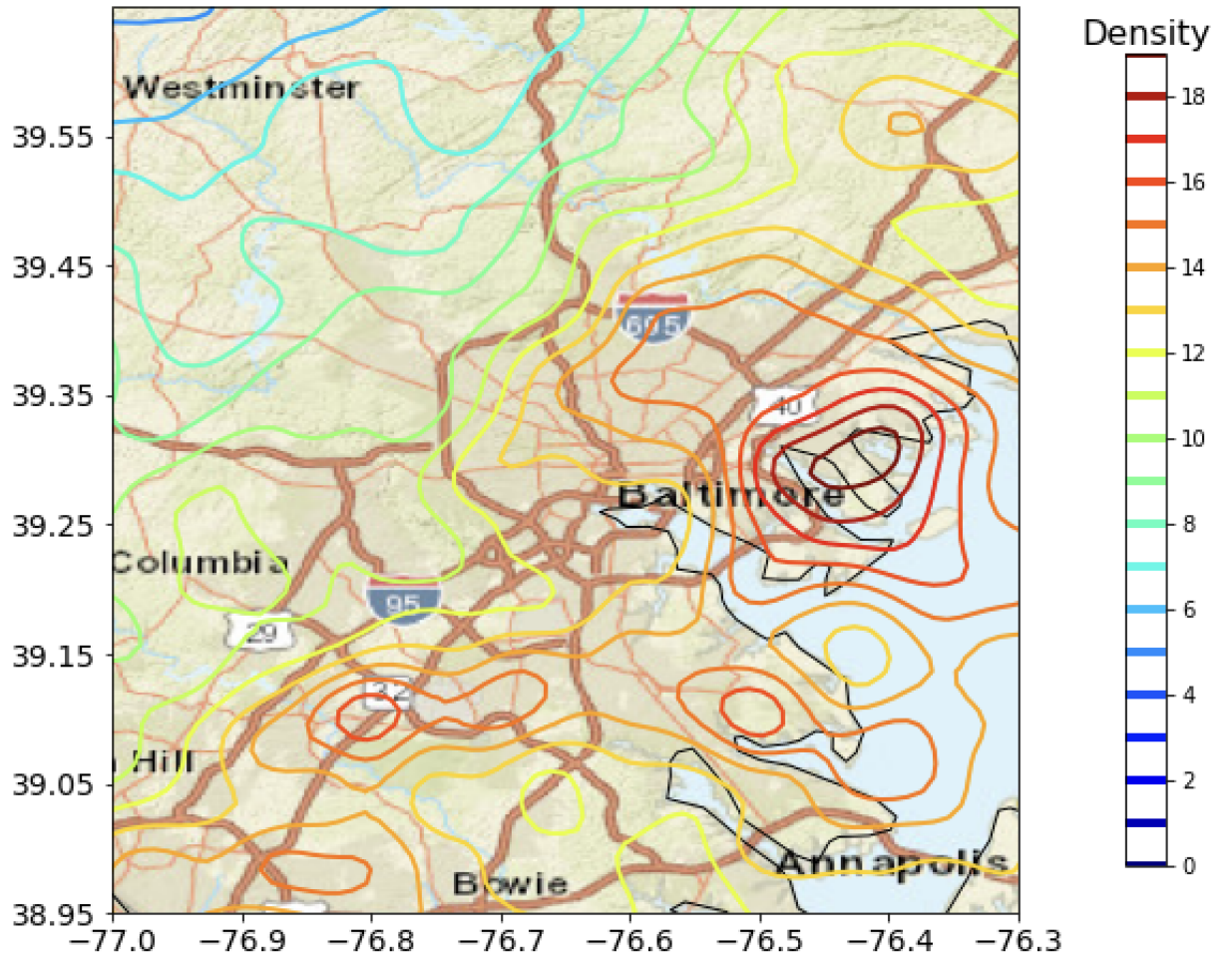


**Figure 5.** Mean annual lightning flash density (strikes  $km^{-2}$  per year) based on NLDN lightning data.



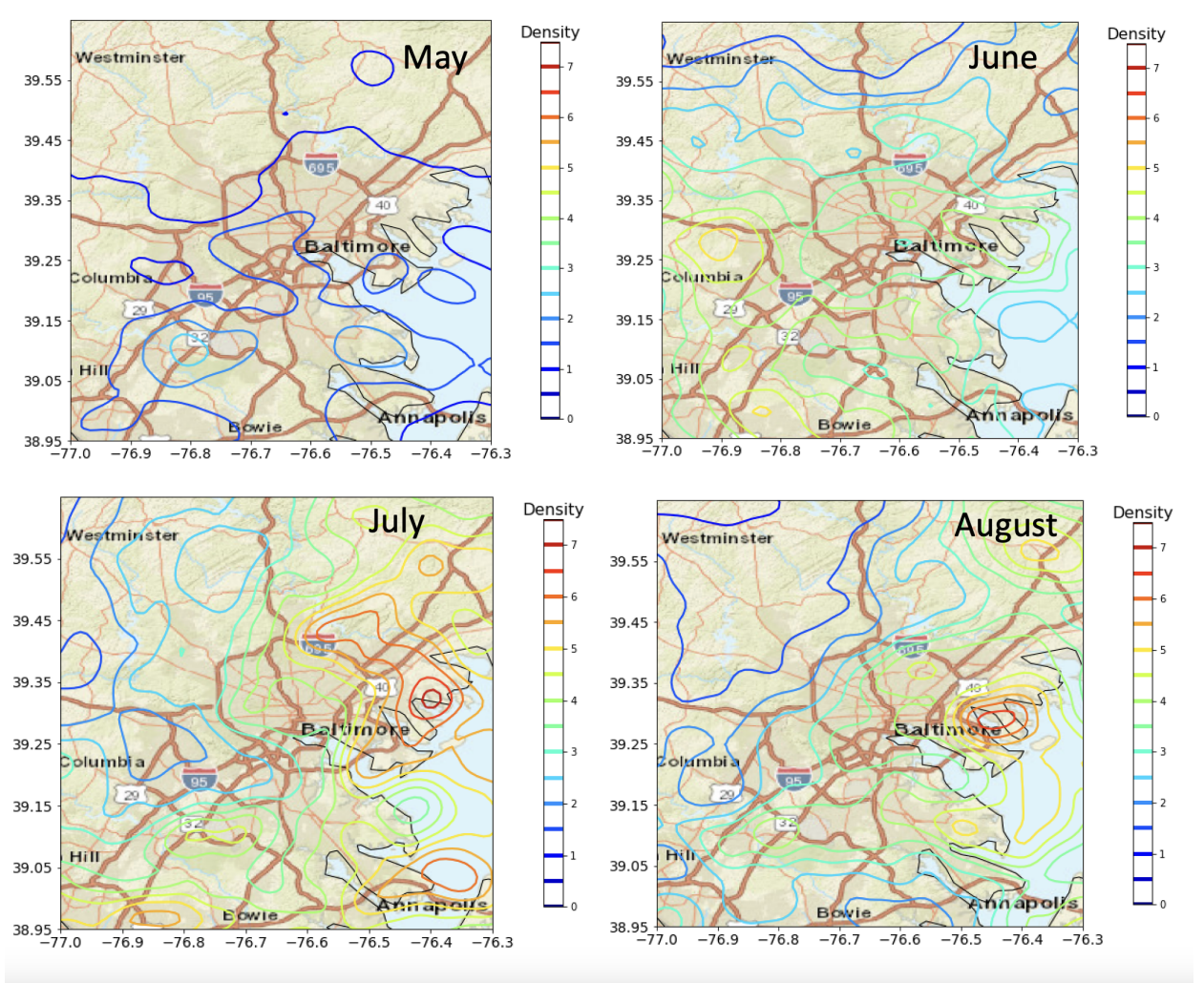


**Figure 6.** Mean monthly lightning flash density (strikes  $km^{-2}$  per month) for May (upper left), June (upper right), July (lower left) and August (lower right).

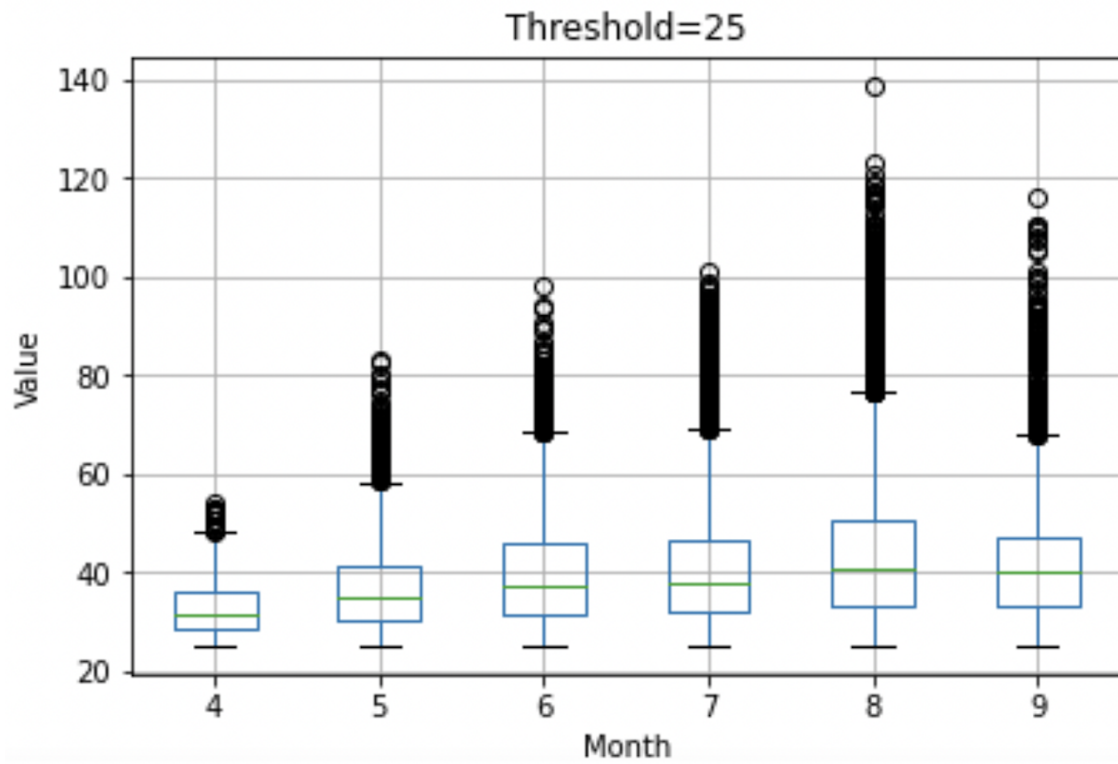


**Figure 7.** Monthly boxplots of annual maximum hourly rainfall, conditioned on the annual maximum exceeding 25 mm. Annual maximum values for all grids are assigned to the month in which they occur.



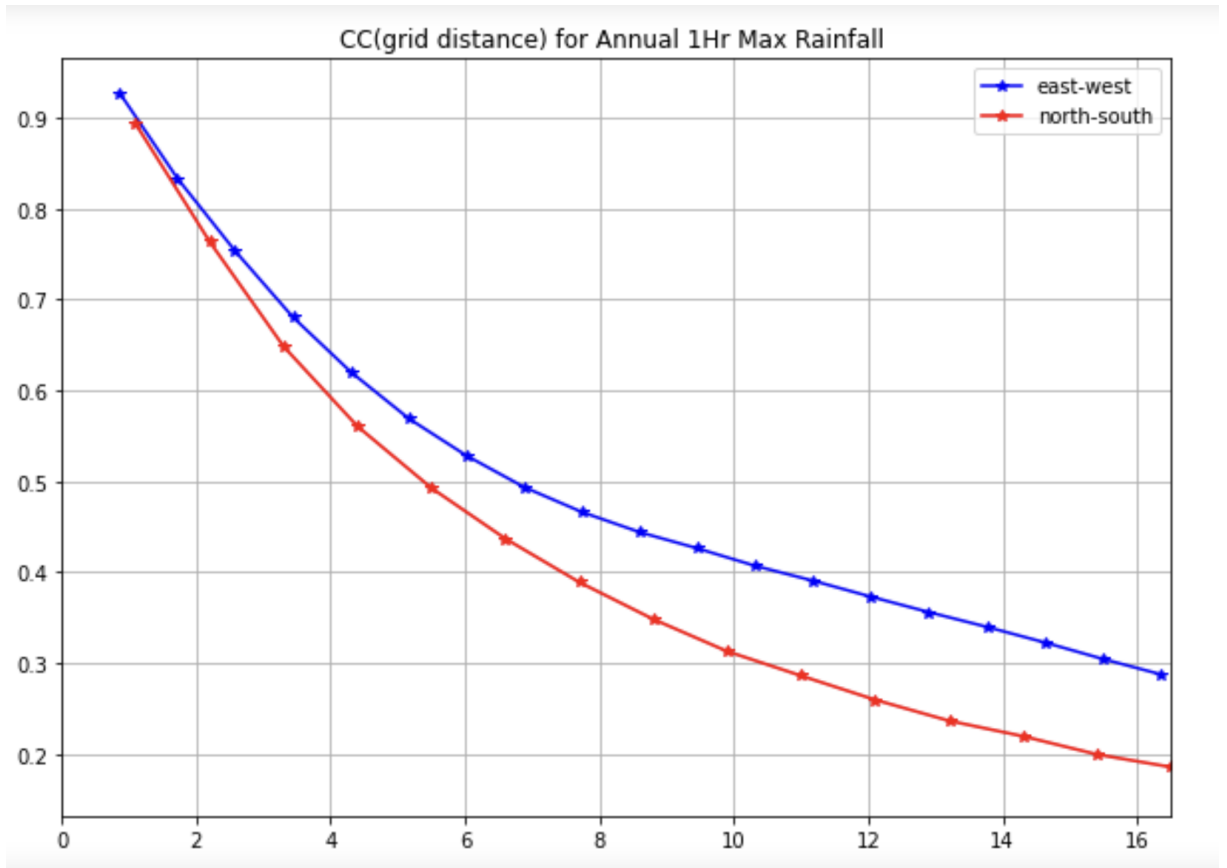


**Figure 8.** Spatial correlation of annual maximum 1 hour rainfall; blue stars for east-west correlation; red stars for north-south correlation.

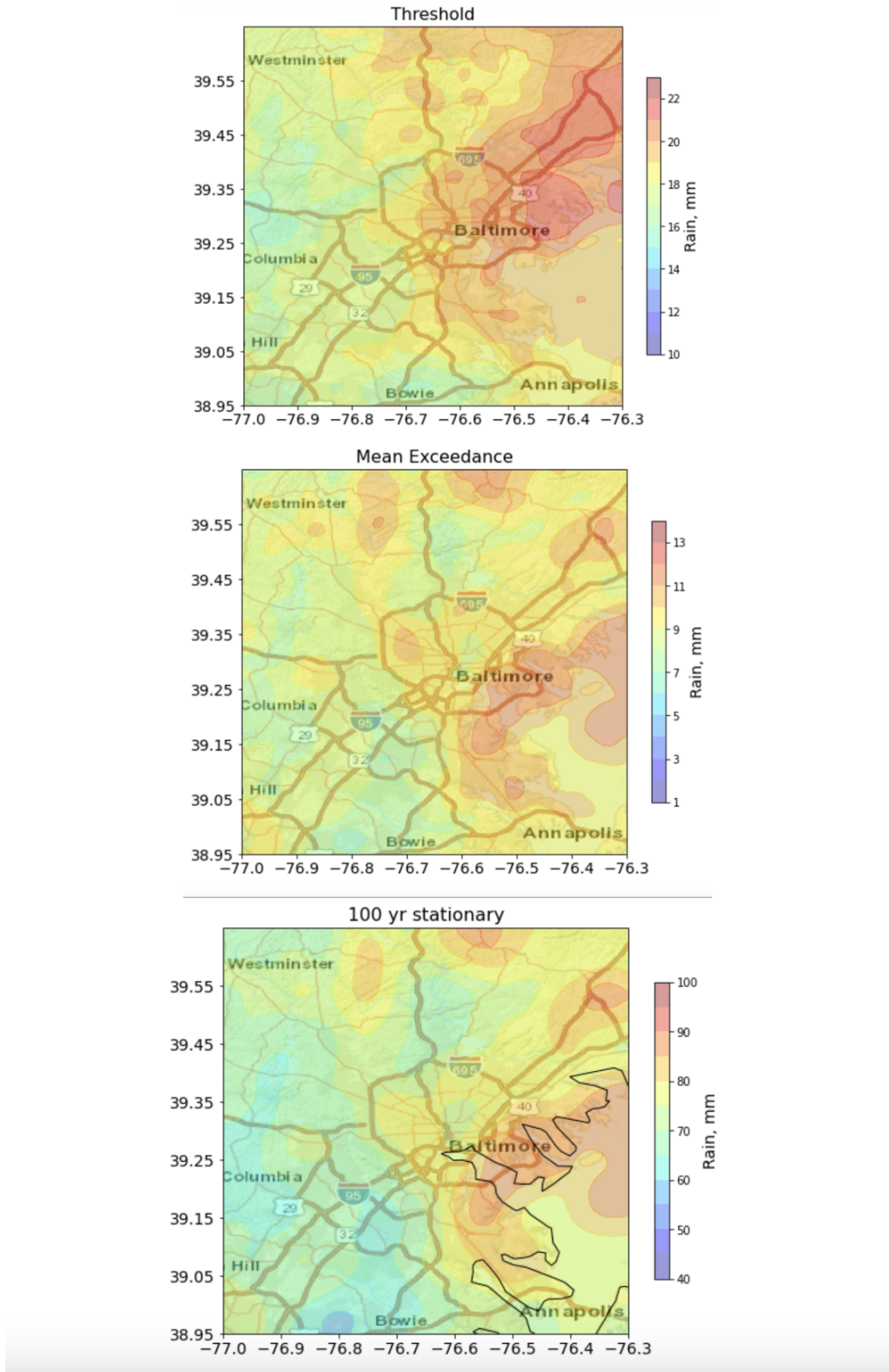


**Figure 9.** Threshold (mm; top) and mean exceedance (mm; middle) for Peaks-over-Threshold model. Bottom panel shows the 100-year hourly rainfall (mm).

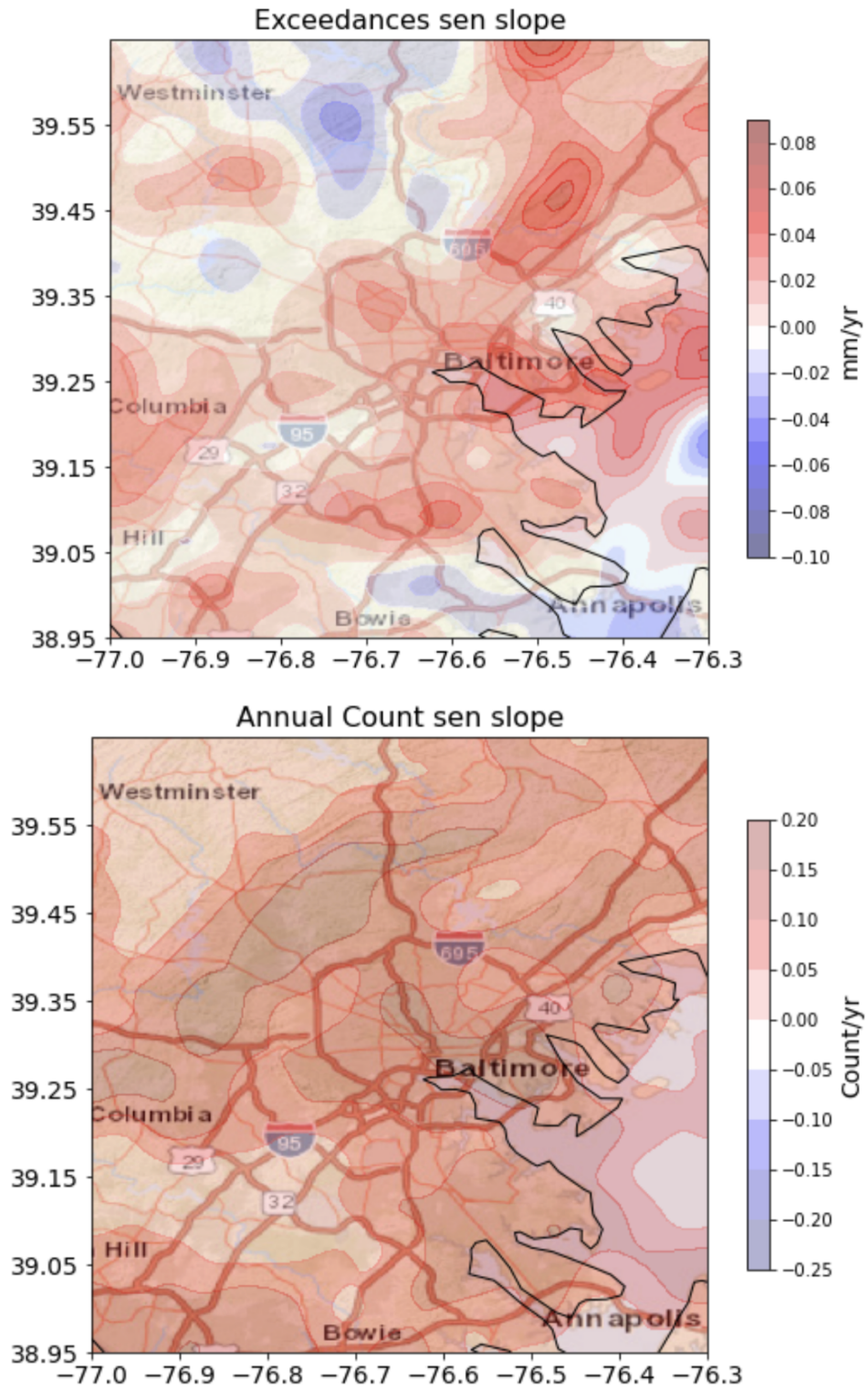


**Figure 10.** Sen slope for mean exceedance (top) and annual counts (bottom).

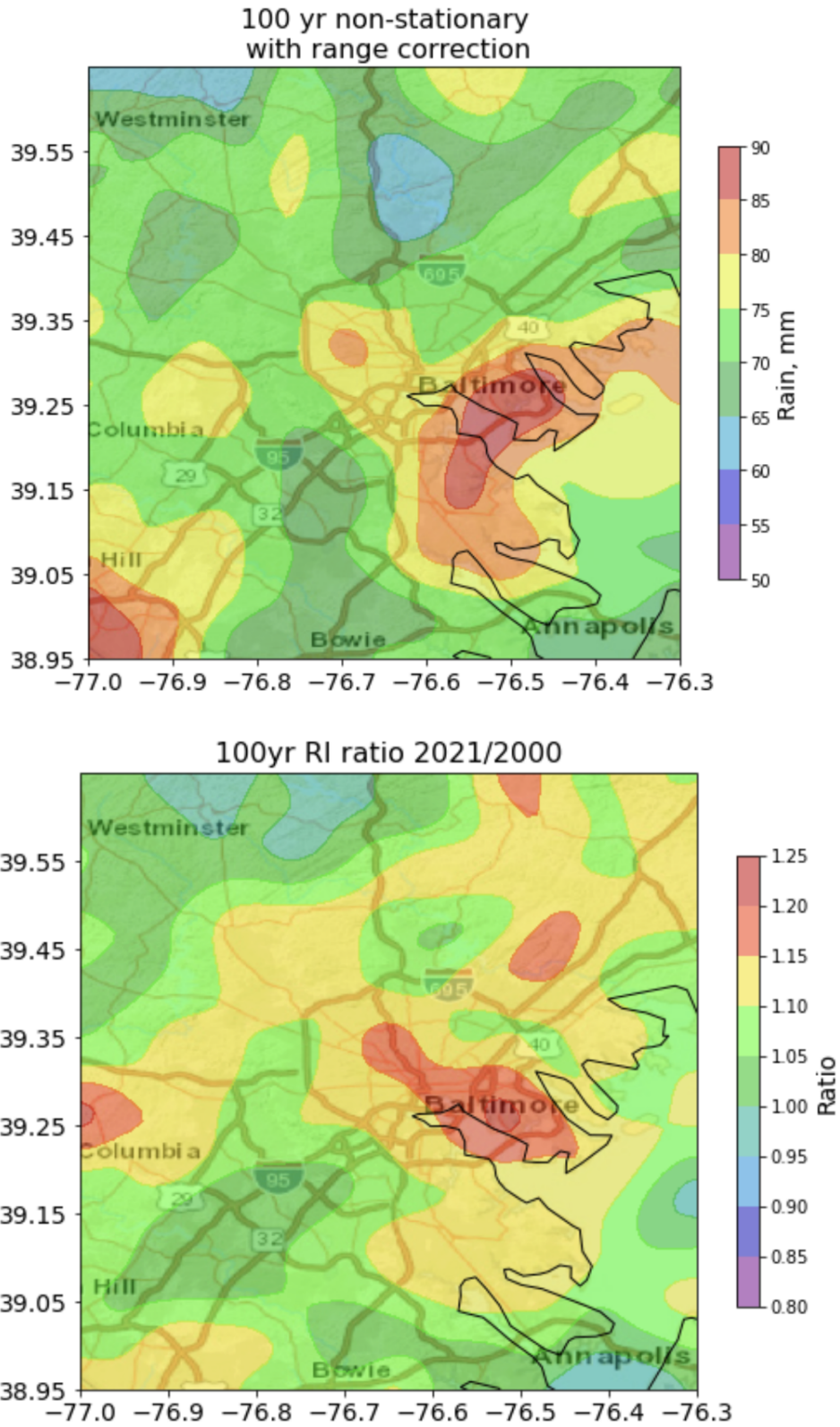


**Figure 11.** 100-year hourly rainfall in 2021 based on POT analyses (top); ratio of 100-year hourly rainfall in 2021 to 2000 (bottom)



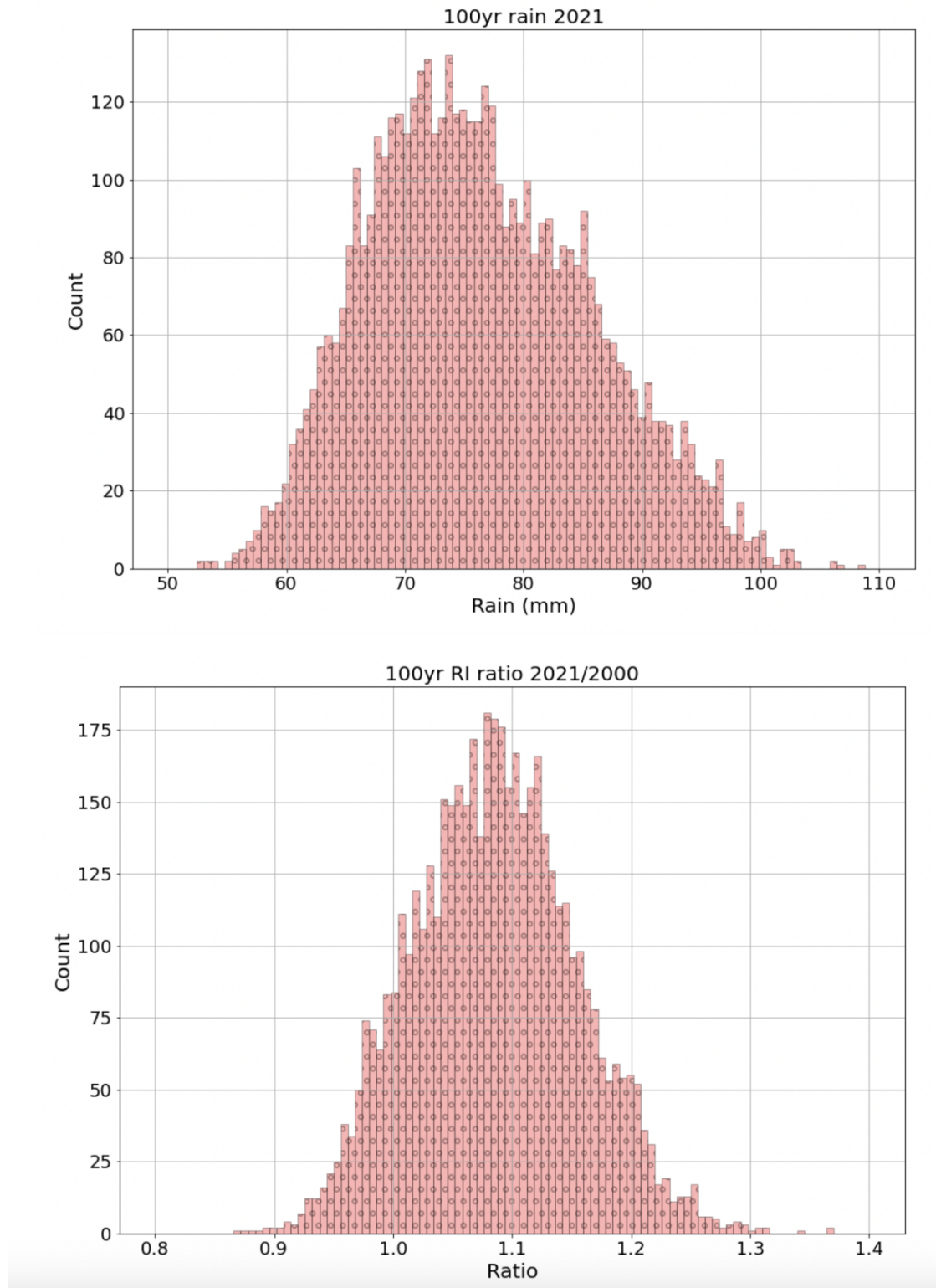


**Figure 12.** Distribution of 100 year, 1 hour rainfall for 2021 (mm; top) and ratio of 2021 100-year hourly rainfall to 2000 100-year hourly rainfall (bottom), based on POT analyses (see Figure 11).

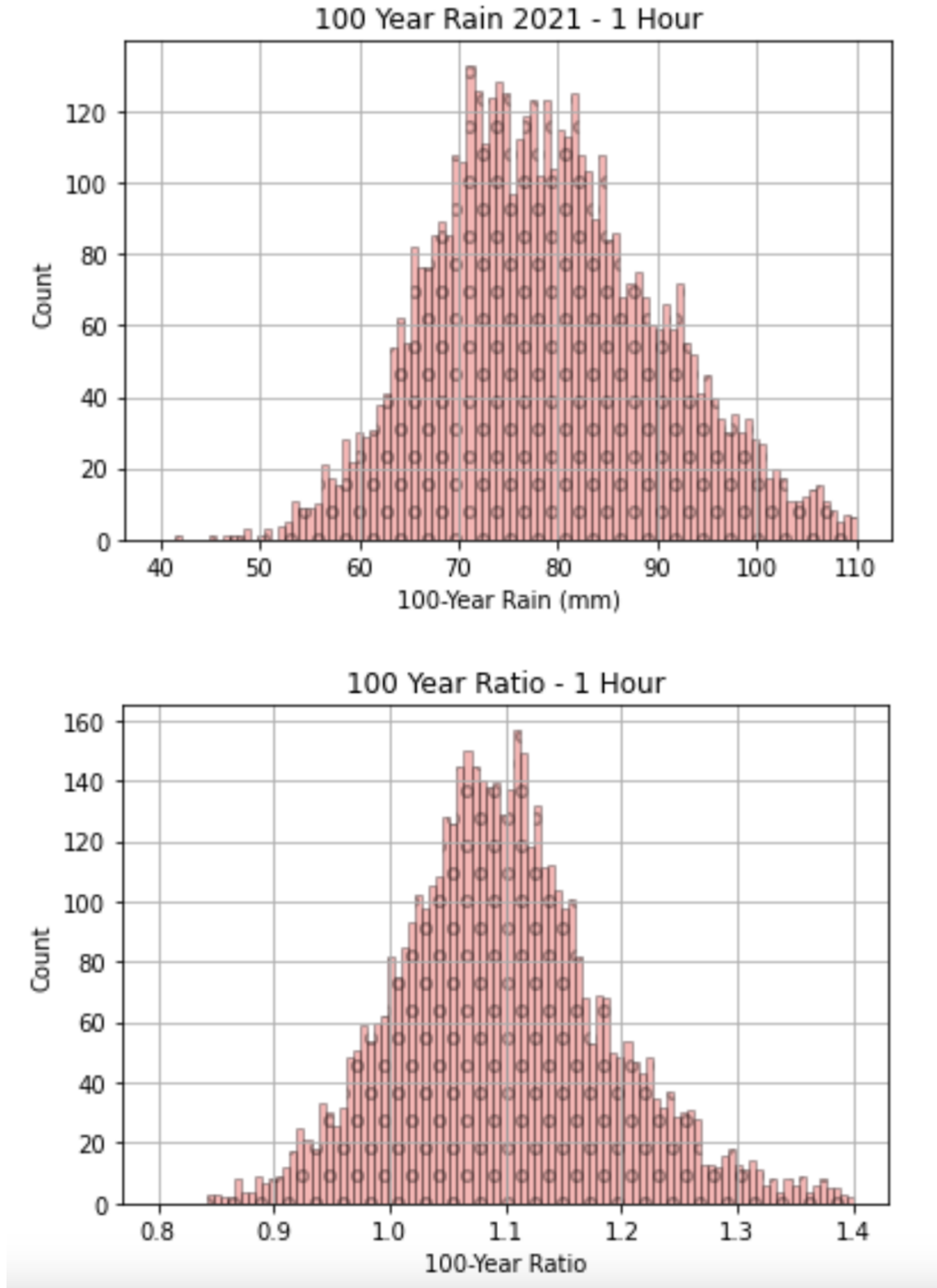


**Figure 13.** Distribution of 100 year, 1 hour rainfall (mm) for the year 2021 (top) and ratio of 100 year rainfall in 2021 to 100 year rainfall in 2000 (bottom), based on annual maximum time series and Gumbel distribution, with location parameter a linear function of year.



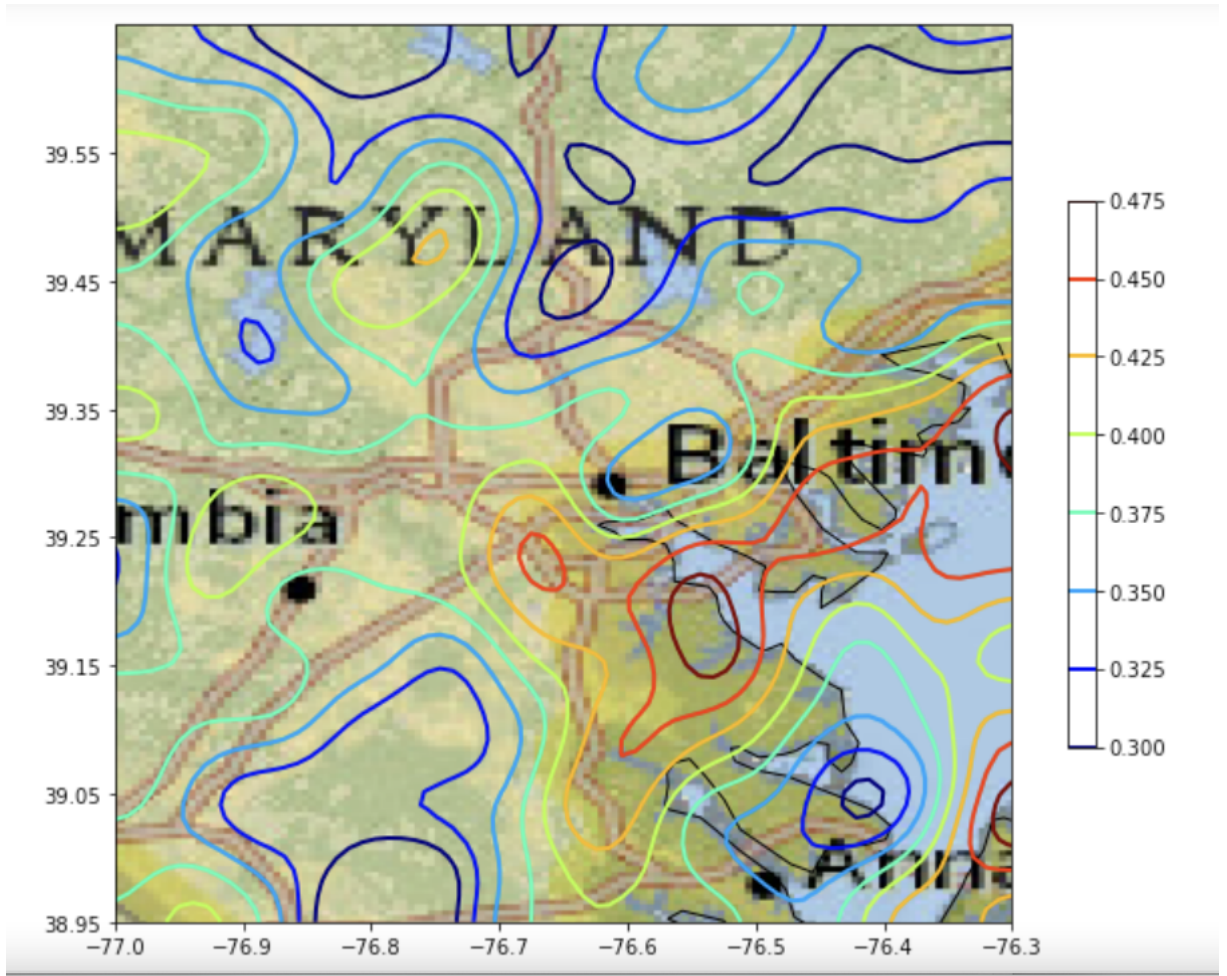


**Figure 14.** Fraction of annual maximum hourly values (from the 22 year record) which occur on the same day as the daily maximum value.

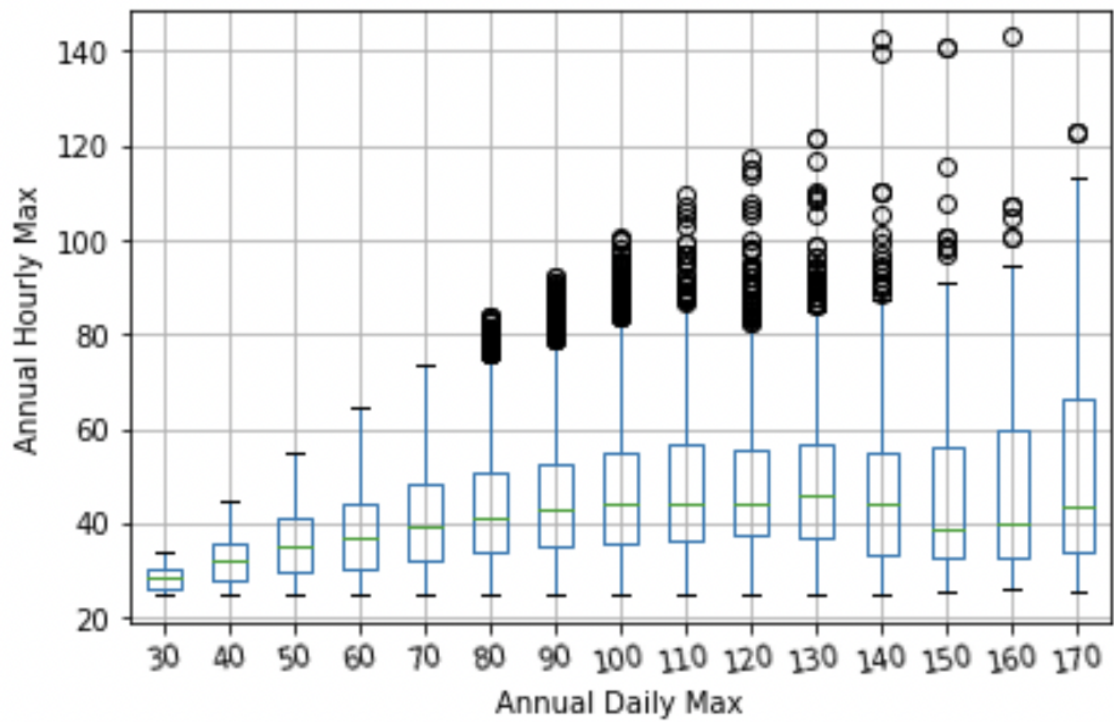


**Figure 15.** Boxplots of annual maximum hourly rainfall for years when the maximum hourly rainfall occurs on the same day as the daily max, conditioned on values of the daily max.

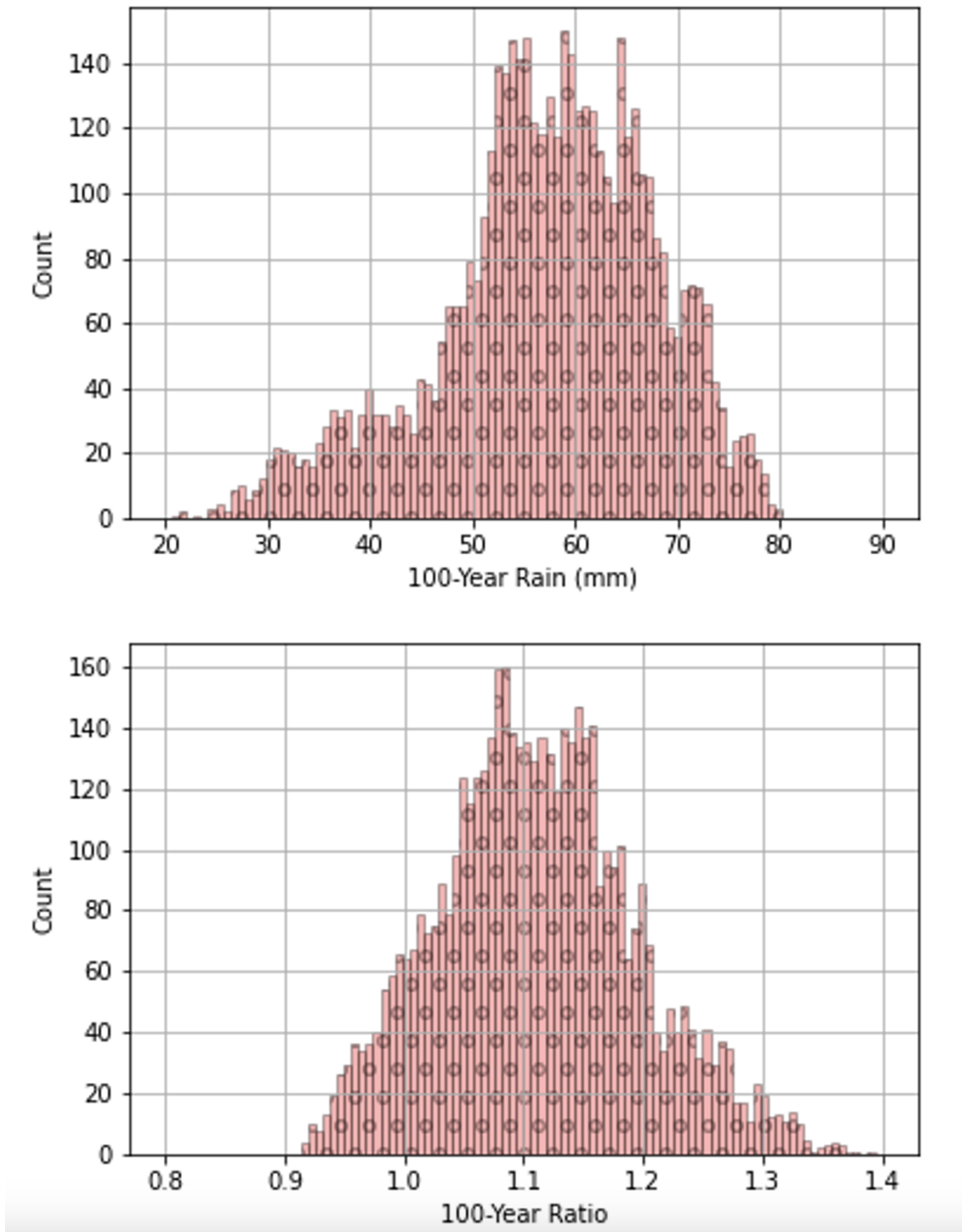


**Figure 16.** Distribution of 100 year, 1 hour rainfall (mm) for the year 2021 at  $100 \text{ km}^2$  (top) and ratio of 100 year rainfall in 2021 to 100 year rainfall in 2000 at  $100 \text{ km}^2$  (bottom).